*J. Fluid Mech.* (2010), *vol.* 664, *pp.* 510–539. 
doi:10.1017/S0022112010003976

# Asymptotic properties of the overall sound pressure level of subsonic jet flows using isotropy as a paradigm

M. Z. AFSAR†

Department of Engineering, University of Cambridge, Cambridge CB3 0DY, UK

(Received 19 November 2008; revised 19 July 2010; accepted 26 July 2010;
first published online 3 November 2010)

Measurements of subsonic air jets show that the peak noise usually occurs when observations are made at small angles to the jet axis. In this paper, we develop further understanding of the mathematical properties of this peak noise by analysing the properties of the overall sound pressure level with an acoustic analogy using isotropy as a paradigm for the turbulence. The analogy is based upon the hyperbolic conservation form of the Euler equations derived by Goldstein (*Intl J. Aeroacoust.*, vol. 1, 2002, p. 1). The mean flow and the turbulence properties are defined by a Reynolds-averaged Navier–Stokes calculation, and we use Green's function based upon a parallel mean flow approximation. Our analysis in this paper shows that the jet noise spectrum can, in fact, be thought of as being composed of two terms, one that is significant at large observation angles and a second term that is especially dominant at small observation angles to the jet axis. This second term can account for the experimentally observed peak jet noise (Lush, *J. Fluid Mech.*, vol. 46, 1971, p. 477) and was first identified by Goldstein (*J. Fluid Mech.*, vol. 70, 1975, p. 595). We discuss the low-frequency asymptotic properties of this second term in order to understand its directional behaviour; we show, for example, that the sound power of this term is proportional to the square of the mean velocity gradient. We also show that this small-angle shear term does not exist if the instantaneous Reynolds stress source strength in the momentum equation itself is assumed to be isotropic for any value of time (as was done previously by Morris & Farrasat, *AIAA J.*, vol. 40, 2002, p. 356). However, it will be significant if the auto-covariance of the Reynolds stress source, when integrated over the vector separation, is taken to be isotropic in all of its tensor suffixes. Although the analysis shows that the sound pressure of this small-angle shear term is sensitive to the statistical properties of the turbulence, this work provides a foundation for a mathematical description of the two-source model of jet noise.

**Key words:** aeroacoustics, jet noise

## 1. Introduction

The existence of different types of mechanisms that contribute to the noise observed in the far field when a jet flow breaks down into turbulent motion has been argued

† Present address: Ohio Aerospace Institute, 22800 Cedar Point Road, Cleveland, OH 44142, USA. Email address for correspondence: mohammed.afsar@cantab.net

for quite some time now. Experiments on subsonic jet flows, both the early studies by Lush (1971) and Ahuja (1973) for example, and even the most recent analysis by Morris (2008, 2009), have shown certain universal features of the overall sound pressure level (OASPL) of a cold jet flow that seem intuitively reasonable. The peak jet noise is seen to occur when the observation point is positioned close to the jet axis, often near 30° (Morris 2008, 2009). At larger observation angles, perpendicular to the jet axis for example, there is an observed drop off in the OASPL. However, these studies also indicate that the peak OASPL for all high-subsonic Mach-number jets is, more or less, independent of Reynolds number.

Most of the mathematical explanations of the jet noise spectrum began with an acoustic analogy (Lighthill 1952). Although the original form of Lighthill's theory gave a reasonable understanding of the jet sound pressure at 90°, the peak jet noise became somewhat difficult to predict within the original acoustic analogy approach for example, especially with the view of developing a unified mathematical model to understand the behaviour of the acoustic spectrum. This difficulty with the original acoustic analogy essentially came about because the base flow velocity about which the fluctuation in pressure was defined was zero. Recently, however, the acoustic analogy approach was generalized by Goldstein (2003) for a completely arbitrary base flow. The standard procedure under the generalized acoustic analogy approach involves re-arranging the Navier–Stokes equations so that a linear differential operator acts on the dependent variables of choice. As Goldstein (2002) pointed out, these dependent variables do not have to be linear themselves, but the differential operator that acts upon them must be, so that a solution (for the pressure variable, say) can be sought using Green's theorem. Any nonlinear terms that involve fluctuations in momentum, or the Reynolds stress, are moved to the right-hand side, and represent the 'generators', or the source terms of the problem, such that these are the quantities about which we have some prior knowledge. Indeed, one of the many advantages of working with the generalized acoustic analogy approach from the outset is that one can recover the classical results. Allowing the base flow to be zero, for example, allows one to recover a Lighthill-type solution and, moreover, by defining the mean flow to be a parallel shear layer in the streamwise direction allows one to recover the next advancement of Lighthill's formalism of the problem, namely Lilley's equation (Lilley 1974).

Lilley's development of the acoustic analogy was not only in the definition of the mean flow for the wave propagation problem. What Lilley (1958) also envisaged was the jet noise spectrum being composed of two terms, a 'self-noise' term that would dominate at large observation angles to the jet axis and would remain relatively directionless, and a 'shear noise' term that depended on the mean-flow-gradient profile (for a jet flow defined by a parallel shear layer) and would be most directional at small observation angles. In fact, it was the analysis of the Lilley's equation that provided a breakthrough in explaining the existence of this shear term. Goldstein (1975) analysed the low-frequency behaviour of the acoustic spectrum using Lilley's equation. He showed that it would remain proportional to the square of the mean velocity gradient, with a directionality factor that peaked at small angles to the jet axis.

However, since Lilley's analysis, many questions still remained open, for example, how one would devise a jet noise model that naturally recovered this shear noise term at small observation angles together with a 'self-noise'-type behaviour at larger observation angles. Part of the difficulty in doing this, however, was that there was never much agreement in the theoretical community about how to define the

shear noise and self-noise terms. So, for example, the definitions used over the years may appear to be quite different from Lilley's original postulate (see, for example, Ribner 1969). In fact, this point was highlighted by Balsa (1977), who explained that artificially decomposing the problem at the very outset into self-noise and shear noise components not only makes the whole analysis become rather complicated, but is not mathematically consistent, because what was originally thought of as contributing mostly to the self-noise term (the fluctuating Reynolds stress source term on the right-hand side of the momentum equation) can have components that are directional.

Indeed, the algebraic complications of using Lilley's equation as the starting point of the analysis were shown in the work of Colonius, Lele & Moin (1997), where, after linearization, the (mathematical) source involved five terms, each having two parts. Although analysis of this source using a direct numerical simulation (DNS) of a two-dimensional compressible mixing layer showed that the Lilley-based acoustic analogy was in good agreement with the acoustic data from the DNS, this complicated mathematical form meant that the source was composed of a very large number of nearly cancelling terms, which made its numerical evaluation difficult (Crighton 1993; Colonius *et al.* 1997; Freund 2001). However, this work did serve to show the benefit of using an approximate form of the Lilley's source term proposed in Goldstein (1976) and later, through an alternative derivation, in Goldstein (1984).

A more extensive diagnostic test of the acoustic analogy was performed by Freund (2001, 2003), who conducted a DNS study of a Mach 0.9, Reynolds number 3600 turbulent jet. The simulation was validated against an experiment by Stromberg, McLaughlin & Troutt (1980) at the same flow conditions (we hereafter refer to this experiment as the Stromberg jet). In Freund (2001), the mean flow and radiated sound were shown to be in good agreement with the data from experiment. There was, however, some concern whether the results from the DNS simulation of this low-Reynolds jet could give understanding of the acoustic properties of higher-Reynolds-number flows. In terms of the mean flow, Freund (2001), and originally Stromberg *et al.* (1980), reported that the flow field had properties common to higher-Reynolds-number turbulent jets (Freund 2001, figure 2), although the potential core length was slightly longer. On the other hand, Freund (2001) explained that low-Reynolds-number jets have acoustic properties that are 'more directive' (see, for example, Mollo-Christensen, Koplin & Martucelli 1964; Lush 1971; Power *et al.* 2004). That is, the OASPL at 90° to the jet axis is lower than it would be for a higher-Reynolds-number jet, at a similar Mach number (which is partly due to the fact that the initial shear layers are laminar in low-Reynolds-number jets). This highly directive behaviour is shown clearly in Stromberg *et al.* (1980, figure 11) and in Freund (2001, figure 10).

An important property that we can infer from the experiments on subsonic jets is that the peak OASPL, which usually occurs at 30° to the jet axis, is relatively independent of Reynolds number. This is shown in Freund (2001, figure 10) and in Bodony & Lele (2008, figure 9*a*). The low-Reynolds-number jet does, therefore, represent a meaningful case for us to understand the peak OASPL, in the context of a two-source description, that is, in the sense that the acoustic spectrum is given (mathematically) by the sum of two terms, one representing the peak noise at small observation angles, with the other term being dominant at larger angles, and this behaviour has been observed even in low-Reynolds-number jet flows. Although Freund (2001) was able to successfully predict the OASPL at 30° for the Stromberg jet, our aim is to provide a mathematical explanation for this peak noise within a two-source description.

The Freund database (2003) was also used to check various approximations that are often made in the acoustic analogy. More recent computational work on jet noise, however, has focused on the use of large eddy simulation (LES). Moore, Slot & Boersma (2007) conducted an LES of a subsonic jet at a very low Reynolds number of 2500 and compared their results to the work of Freund (2001). LES-based jet noise analysis and prediction have been performed successfully by a number of researchers, especially in predicting the peak jet noise, for example, Anderssen (2003), Bodony & Lele (2005), Wu *et al.* (2005), Shur, Strelets & Spalart (2007), Mosedale & Drikakis (2007) and Bodony & Lele (2008) to name a few. The technical issues involved in the LES-based prediction schemes can be found in Colonius & Lele (2004), Bodony (2004) and Wang, Freund & Lele (2006).

A mathematical explanation of the OASPL using the acoustic analogy is not the only starting point for the jet noise problem. Tam *et al.* (2008) developed an alternative theory for the jet noise spectrum based on a semi-empirical model described in Tam & Auriault (1999) for the high frequencies and an instability wave model. The idea of using an instability wavepacket to describe the breakdown of the coherent structures in terms of the growth-stabilization-decay cycle has been around for decades now (see the review by Tam 1995). For example, Bishop, Ffowcs-Williams & Smith (1971), Tam (1971), Crow (1972), Ffowcs-Williams & Kempton (1978), Liu & Merkine (1976), Alper & Liu (1978), Liu & Mankbadi (1984), Huerre & Crighton (1983) and Tam & Burton (1984). In the most recent work under this premise, Wu & Huerre (2009) showed that an instability wavepacket modulated simultaneously in space and time radiates low-frequency sound waves in a manner similar to that found by Goldstein (1975).

In this paper, we re-analyse the jet noise problem and show that the OASPL of a cold jet flow can be understood to a reasonable level by two mathematical terms using isotropy as a paradigm for the kinematics of the turbulence. One of these terms is significant at large observation angles, while the second term is the 'shear term' because it is proportional to the local mean velocity gradient. We show that this shear term is most dominant at small observation angles to the jet axis and has similar properties to those found by Goldstein (1975). These two terms can then be thought of as the 'self-noise' and 'shear noise' terms in the spirit of Lilley (1958), but what is important here is that we do not introduce this decomposition at any point in the analysis, and show by remaining consistent with the assumptions that these terms naturally appear in the power spectral density formula.

We show that the shear term will actually exist if the auto-covariance of the fluctuating Reynolds stress source term, when integrated over the vector separation, is taken to be isotropic in all of its tensor suffixes. However, this shear term will not occur if the instantaneous Reynolds stress source strength is itself taken to be isotropic, as was done previously by Morris & Farrasat (2002), and implicitly assumed in the work of Goldstein & Leib (2005). But we show that the sound pressure of these terms will depend crucially on the statistical properties of the turbulence (length scale and time scale parameters in a particular functional form of the longitudinal correlation function). The acoustic analogy we use to analyse the problem is based upon the hyperbolic conservation form of the linearized Euler equations that Goldstein (2002) derived, and we solve the wave propagation problem for a mean flow based upon a parallel shear-layer model. The source statistics and mean flow are given by a Reynolds-averaged Navier–Stokes (RANS) calculation of the Stromberg jet (Wu *et al.* 2005; J. J. McGuirk, private communication) and we focus on calculating the OASPL only, which we compare with experiment.

## 2. Acoustic analogy

The basic acoustic analogy equations are based upon the following four fundamental theoretical statements (Lighthill 1952; Goldstein 2002, 2003, 2005; Goldstein & Leib 2008; Afsar 2008).

(*a*) The region of turbulence is localized within the jet and the fluid at infinity is at rest. The turbulence field itself will be described through a 'source term', which is simply a stationary random function of the space–time coordinates $(\boldsymbol{y}, \tau)$.

(*b*) Acoustic motions are weak mechanical disturbances that propagate from the flow by transferring momentum to the fluid in their immediate vicinity (Feynman, Leighton & Sands 1964). Hence, we can divide the fluid-mechanical variables in the Navier–Stokes equations into their mean and fluctuating components.

(*c*) The acoustic pressure ($p_{acoustic}$) is then defined by the simple equation:

$$p_{acoustic} = \lim_{|\boldsymbol{x}|\to\infty} p(\boldsymbol{x}, t), \tag{2.1}$$

where $(\boldsymbol{x}, t)$ is the observation point.

(*d*) The fluid-mechanical variables do not need to be linear so long as (2.1) is satisfied. For example, in Goldstein (2003) and Goldstein & Leib (2008), a nonlinear pressure variable is used, but (2.1) is still, of course, satisfied. Moreover, since the Navier–Stokes can be rewritten as a formally linear set of equations for a residual component (defined relative to the base flow), a general solution for $p_{acoustic}$ can be posed using the adjoint Green's function (Goldstein 2002).

### 2.1. *Basic equations*

In this paper, we use an earlier form of the linearized Navier–Stokes equations shown in Goldstein (2002), where the pressure variable is already linear. We begin by deriving the formula for the power spectral density of the pressure fluctuation at the field point $(\boldsymbol{x}, t)$, due to turbulence at $(\boldsymbol{y}, \tau)$. We take the customary step of neglecting the noise due to viscous dissipation and heat conduction, which are known to make an insignificant contribution to the acoustic field when the turbulence is on a terrestrial scale (Crighton 1969). Further evidence to support this came from the direct numerical simulation (DNS) study of Colonius & Freund (2000) and Freund (2003), both of whom showed that the contribution of the viscous stress tensor to the acoustic field was negligible, even down to a Reynolds number of 2000.

The Euler equations that result can be rewritten in terms of this arbitrary base flow and residual component, both of which can be unsteady (Goldstein 2002). But since we are going to perform noise calculations using a steady RANS solution, it makes sense to choose the base flow to be the time-averaged mean field and write them in the field variables $(\boldsymbol{y}, \tau)$ because the turbulence is confined to the jet flow only. With that in mind, we introduce the usual notation for the averaging operations: the overbar to represent the time average (with the single prime being its perturbation) and the tilde for the Favre average (with the double prime being its perturbation). Hence

$$\overline{u}(\boldsymbol{y}) \equiv \lim_{T\to\infty} \frac{1}{2T} \int_{-T}^{T} u(\boldsymbol{y}, \tau)\, \mathrm{d}\tau \tag{2.2}$$

and

$$\overline{\rho}\widetilde{u} \equiv \overline{\rho u}. \tag{2.3}$$

Here, $T$ is the time period of averaging, and $\overline{u'} = 0$. The linearized Euler equations that now follow are defined about the mean flow field: density $\bar{\rho}(\boldsymbol{y})$, pressure $\bar{p}(\boldsymbol{y})$ and velocity $\tilde{v}_j(\boldsymbol{y})$. However, as Goldstein (2002) showed, this system of equations can be

rewritten as a hyperbolic conservation form by introducing a nonlinear momentum variable, $u_i(\boldsymbol{y},\tau)=\rho v_i''(\boldsymbol{y},\tau)$, that has zero time average. Throughout this paper, we apply the standard tensor convention of summation across repeated suffixes. Here, $\gamma$ is the ratio of the specific heat capacities of air. The equations for mass, momentum and energy are then given by

$$\frac{\partial \rho'}{\partial \tau}+\frac{\partial}{\partial y_j}(\rho'\tilde{v}_j+u_j)=0, \tag{2.4}$$

$$\frac{\partial u_i}{\partial \tau}+\frac{\partial}{\partial y_j}(\tilde{v}_j u_i)+\frac{\partial p'}{\partial y_i}+u_j\frac{\partial \tilde{v}_i}{\partial y_j}-\left(\frac{\rho'}{\bar{\rho}}\right)\frac{\partial \tilde{\tau}_{ij}}{\partial y_j}=\frac{\partial T'_{ij}}{\partial y_j},\quad i=1,\ldots,3, \tag{2.5}$$

$$\frac{1}{(\gamma-1)}\frac{\partial p'}{\partial \tau}+\frac{1}{(\gamma-1)}\frac{\partial}{\partial y_j}(p'\tilde{v}_j)+p'\frac{\partial \tilde{v}_j}{\partial y_j}+\frac{\partial}{\partial y_j}(u_j\tilde{h})-\frac{u_i}{\bar{\rho}}\frac{\partial \tilde{\tau}_{ij}}{\partial y_j}=Q'. \tag{2.6}$$

In this system of equations, the Favre-averaged stagnation enthalpy and its perturbation take the special definitions $\tilde{h}_0=\tilde{h}+(1/2)\tilde{v}^2$ and $h_0''=h''+\tilde{v}_i v_i''+(1/2)v''^2$. The second-rank tensor $\tilde{\tau}_{ij}$ on the left-hand side in linearized equations (2.5) and (2.6) is defined by the equation $\tilde{\tau}_{ij}=\delta_{ij}\bar{p}+\bar{\rho}\widetilde{v_i''v_j''}$. Using the time-averaged momentum equation, however, we can rewrite it as $\tilde{v}_j(\partial\tilde{v}_i/\partial y_j)=-(1/\bar{\rho})(\partial\tilde{\tau}_{ij}/\partial y_j)$, which shows that if the mean flow is approximated by a parallel shear layer, with $\tilde{v}_j(\boldsymbol{y})=\delta_{j1}U(y_2,y_3)$, the vector $\partial\tilde{\tau}_{ij}/\partial y_i$ will be identically zero. Hence, $\partial\tilde{\tau}_{ij}/\partial y_i$ is a term associated with non-parallel mean-flow effects, and therefore it will remain at most an $O(\epsilon)$ term for a jet flow spreading with a spread rate $\epsilon$ (Goldstein & Leib 2005). The term on the right-hand side of the energy equation depends not only on momentum transfer through the Reynolds-stress fluctuations, but also on stagnation enthalpy fluctuations. Recent numerical evidence by Bodony & Lele (2008) and Bodony (2009) suggests that density fluctuations could be sizeable even for cold jet flows, particularly for jet Mach numbers greater than 0.9. However, since our aim here is to highlight the shear term and that could explain the peak jet noise, and which originates from momentum transfer, we neglect the stagnation enthalpy contribution (even though it contains a term linear in the velocity fluctuation) and density fluctuations. Hence, we allow $\rho(\boldsymbol{y},\tau)\approx\rho(\boldsymbol{y})$. The terms on the right-hand side of the linearized equations then reduce to

$$T'_{ij}(\boldsymbol{y},\tau)=-\bar{\rho}(\boldsymbol{y})\left[v_i''v_j''(\boldsymbol{y},\tau)-\widetilde{v_i''v_j''}(\boldsymbol{y})\right], \tag{2.7}$$

$$Q'(\boldsymbol{y},\tau)=-\tilde{v}_j(\boldsymbol{y})\frac{\partial T'_{ij}}{\partial y_i}(\boldsymbol{y},\tau)+\frac{1}{2}\delta_{ij}\left[\frac{\mathrm{D}T'_{ij}}{\mathrm{D}\tau}(\boldsymbol{y},\tau)+\frac{\partial \tilde{v}_k}{\partial y_k}(\boldsymbol{y})T'_{ij}(\boldsymbol{y},\tau)\right]. \tag{2.8}$$

Here, $\mathrm{D}/\mathrm{D}\tau$ is the usual convective derivative given by $\mathrm{D}/\mathrm{D}\tau=\partial/\partial\tau+\tilde{v}_j(\boldsymbol{y})(\partial/\partial y_j)$.

It is important to realize now that the only source term present in the analysis is $T'_{ij}(\boldsymbol{y},\tau)$, since the term $Q'(\boldsymbol{y},\tau)$ is a function of $T'_{ij}(\boldsymbol{y},\tau)$ as well. Notice that the source term now is purely quadratic in its fluctuation, and should therefore avoid issues associated with sensitivity of its numerical determination (Colonius *et al.* 1997). Equation (2.7) represents the noise due to fluctuating momentum (which we call momentum transfer), and (2.8) involves its interaction with the mean flow, which causes changes of energy to occur (the energy exchange term).

### 2.2. *Solution for the pressure fluctuation*

The solution of the formally linear equations for the pressure variable ($p'$) can be found at a field point outside the jet flow ($\boldsymbol{x}, t$) using Green's theorem. This method has been used many times in the past, for example, the work by Dowling, Ffowcs Williams & Goldstein (1978), Tam & Auriault (1998) and most recently, Goldstein & Leib (2008). The adjoint Green's function must then satisfy a set of adjoint linearized equations that are homogeneous (right-hand side is zero) in the jet region. Any unknown constants in the Green's function solution are easily found, because the Green's function in the jet must reduce to the solution of the wave equation in the far field (the outer region), where the mean flow is all zero.

We use Green's theorem (Morse & Feshbach 1953, pp. 878–886) to express the pressure in terms of an integral over the tensor product of the adjoint vector Green's function and the sources on the right-hand side of (2.7) and (2.8). We assume that the surface terms can be neglected, so that by taking Fourier transforms we get

$$\hat{p}(\boldsymbol{x},\omega) = -\int_{V_\infty(\boldsymbol{y})} \left[ \hat{G}_i(\boldsymbol{y},-\omega \mid \boldsymbol{x}) \frac{\partial \hat{T}_{ij}}{\partial y_j}(\boldsymbol{y},\omega) + \hat{G}_4(\boldsymbol{y},-\omega \mid \boldsymbol{x}) \hat{Q}(\boldsymbol{y},\omega) \right] \mathrm{d}^3\boldsymbol{y}. \tag{2.9}$$

Here, $\hat{T}_{ij}(\boldsymbol{y},\omega)$ is the Fourier transform of $T'_{ij}(\boldsymbol{y},\tau)$ and $\hat{G}_{0,1,2,3,4}(\boldsymbol{y},\omega \mid \boldsymbol{x})$, the Fourier transform of the adjoint Green's function, satisfies the adjoint equations:

$$\mathrm{i}\omega\hat{G}_0 + \tilde{v}_j \frac{\partial \hat{G}_0}{\partial y_j} - \hat{G}_i \tilde{v}_k \frac{\partial \tilde{v}_i}{\partial y_k} = 0, \tag{2.10}$$

$$\mathrm{i}\omega\hat{G}_i + \tilde{v}_j \frac{\partial \hat{G}_i}{\partial y_j} + \frac{\partial \hat{G}_0}{\partial y_i} - \hat{G}_k \frac{\partial \tilde{v}_k}{\partial y_i} + \tilde{h} \frac{\partial \hat{G}_4}{\partial y_i} - \hat{G}_4 \tilde{v}_k \frac{\partial \tilde{v}_i}{\partial y_k} = 0, \quad i = 1,\ldots,3, \tag{2.11}$$

$$\frac{\mathrm{i}\omega}{(\gamma-1)}\hat{G}_4 + \frac{\tilde{v}_j}{(\gamma-1)} \frac{\partial \hat{G}_4}{\partial y_j} - \hat{G}_4 \frac{\partial \tilde{v}_j}{\partial y_j} + \frac{\partial \hat{G}_j}{\partial y_j} = \delta(\boldsymbol{y}-\boldsymbol{x}). \tag{2.12}$$

Here, $\hat{G}_0$ is the adjoint density-like variable and $\hat{G}_1$–$\hat{G}_3$ are the adjoint momentum-like variables. Also, $\hat{G}_4$, the pressure-like quantity, is the variable in the adjoint energy equation (where we have used $\tilde{v}_j(\partial\tilde{v}_i/\partial y_j) = -(1/\overline{\rho})\partial\tilde{\tau}_{ij}/\partial y_j$). At this stage in the analysis, the adjoint Green's functions themselves remain otherwise unrestricted and satisfy any strict definition of causality.

### 2.3. *Equivalent statement*

Our focus in this paper is really the analysis of the source term. As we mentioned before, the only source term in the set-up of the problem now is $\hat{T}_{ij}(\boldsymbol{y},\omega)$. Since it is continuous throughout the field space, we can integrate (2.9) by parts. It seems sensible to do this. Computing spatial derivatives of a function that we can, at best, model, would be numerically challenging, especially given that one would be relying upon a computational fluid dynamics (CFD) solution that is only ever known on a discrete set of points. The Green's function, on the other hand, can be determined, and differentiated, with accuracy. Substituting (2.8) into (2.9) and integrating each term by parts so that we isolate $T_{ij}$ gives an equivalent statement of Green's theorem, the Fourier transform of which is given by

$$\hat{p}(\boldsymbol{x},\omega) = \int_{V_\infty(\boldsymbol{y})} \hat{I}_{ij}(\boldsymbol{y},-\omega \mid \boldsymbol{x}) \hat{T}_{ij}(\boldsymbol{y},\omega)\, \mathrm{d}^3\boldsymbol{y}. \tag{2.13}$$

The components of the second-rank wave propagation tensor, $\hat{I}_{ij}$, are defined by

$$\hat{I}_{ij}(\boldsymbol{y},\omega\mid\boldsymbol{x})=\frac{\partial\hat{G}_j}{\partial y_i}(\boldsymbol{y},\omega\mid\boldsymbol{x})-\left[\frac{\partial\tilde{v}_j}{\partial y_i}(\boldsymbol{y})\hat{G}_4(\boldsymbol{y},\omega\mid\boldsymbol{x})+\tilde{v}_j(\boldsymbol{y})\frac{\partial\hat{G}_4}{\partial y_i}(\boldsymbol{y},\omega\mid\boldsymbol{x})\right]+\frac{\delta_{ij}}{2}\left[\mathrm{i}\omega\left(1+\frac{\tilde{v}_k}{\mathrm{i}\omega}\frac{\partial}{\partial y_k}\right)\hat{G}_4(\boldsymbol{y},\omega\mid\boldsymbol{x})\right]. \quad (2.14)$$

This form of the pressure fluctuation ((2.13) and (2.14)) is similar to (4.6) in Goldstein & Leib (2005). Even though the stationary random function $T'_{ij}$ is not a square-integrable function, and does not, therefore, possess a Fourier transform, this does not pose a problem here because the Fourier transform of its auto-covariance does exist. One further technical point to note here is that although we have taken the usual step and neglected the surface-term contribution that arises from the integration by parts process, what we are taking for granted is that $T'_{ij}(\boldsymbol{y},\tau)$ must decay faster than $|\boldsymbol{y}|^{-2}$ as $|\boldsymbol{y}|\to\infty$. Since if the surface that bounds the volume $V_\infty(\boldsymbol{y})$ is denoted by $S_\infty(\boldsymbol{y})$, and if $S_\infty$ is defined by $s(\boldsymbol{y})=0$, then at any point in $\boldsymbol{y}$, we can define an outward pointing unit normal to $S_\infty$ by $\boldsymbol{n}(\boldsymbol{y})=\nabla s(\boldsymbol{y})/|\nabla s(\boldsymbol{y})|$. Now integrating the momentum transfer term in (2.9), for example, would result in a surface term of the form

$$\int_\tau\int_{S_\infty(\boldsymbol{y})}n_j\left[T'_{ij}(\boldsymbol{y},\tau)G_i(\boldsymbol{y},\tau\mid\boldsymbol{x},t)\right]\mathrm{d}S\,\mathrm{d}\tau, \quad (2.15)$$

which tends to zero if $T'_{ij}(\boldsymbol{y},\tau)$ remains $o(1/|\boldsymbol{y}|^2)$ as $|\boldsymbol{y}|\to\infty$. For an incompressible field, Crow (1970) showed that this condition is easily satisfied. In all other cases, however, we have to rely on the phase cancellations within $T'_{ij}$ to ensure convergence (Goldstein 1976). But, nonetheless, we can identify the transfer of momentum and energy exchange terms within the wave propagation tensor $\hat{I}_{ij}$ commensurate with our definition in § 2.1, i.e.

$$\hat{I}_{ij}(\boldsymbol{y},\omega\mid\boldsymbol{x})=\underbrace{\frac{\partial\hat{G}_j}{\partial y_i}(\boldsymbol{y},\omega\mid\boldsymbol{x})}_{\text{Momentum transfer: term I}}\underbrace{-\left[\frac{\partial\tilde{v}_j}{\partial y_i}(\boldsymbol{y})\hat{G}_4(\boldsymbol{y},\omega\mid\boldsymbol{x})+\tilde{v}_j(\boldsymbol{y})\frac{\partial\hat{G}_4}{\partial y_i}(\boldsymbol{y},\omega\mid\boldsymbol{x})\right]}_{\text{Energy exchange: terms IIa and IIb}}+\frac{\delta_{ij}}{2}\underbrace{\left[\mathrm{i}\omega\left(1+\frac{\tilde{v}_k}{\mathrm{i}\omega}\frac{\partial}{\partial y_k}\right)\hat{G}_4(\boldsymbol{y},\omega\mid\boldsymbol{x})\right]}_{\text{Energy exchange: terms IIIa}}. \quad (2.16)$$

### 2.4. *Power spectral density formula*

The power spectral density of the far-field pressure is

$$\hat{P}(\boldsymbol{x},\omega)=\int_{V_\infty(\boldsymbol{y})}\int_{\boldsymbol{\eta}}\hat{I}^{sym}_{ijkl}(\boldsymbol{y},\boldsymbol{\eta},\omega\mid\boldsymbol{x})\hat{R}_{ij,kl}(\boldsymbol{y},\boldsymbol{\eta},\omega)\,\mathrm{d}^3\boldsymbol{\eta}\,\mathrm{d}^3\boldsymbol{y}, \quad (2.17)$$

where $\boldsymbol{\eta}$ is the vector separation between the correlation positions $\boldsymbol{y}$ and $\boldsymbol{y}+\boldsymbol{\eta}$; in a Cartesian system of coordinates, for example, $\boldsymbol{\eta}=(\eta_1,\eta_2,\eta_3)$. The integrand involves the inner tensor product of two fourth-rank tensors. The wave propagation tensor $\hat{I}^{sym}_{ijkl}$ is defined by the symmetric components of the outer tensor product, $\hat{I}^{sym}_{ij}(\boldsymbol{y},\omega\mid\boldsymbol{x})\hat{I}^{sym}_{kl}(\boldsymbol{y}+\boldsymbol{\eta},-\omega\mid\boldsymbol{x})$, where the symmetric second-rank tensor is defined in the usual way, $\hat{I}^{sym}_{ij}=[\hat{I}_{ij}+\hat{I}_{ji}]/2$. Here, $\hat{R}_{ij,kl}(\boldsymbol{y},\boldsymbol{\eta},\omega)$ is the Fourier transform of the

auto-covariance of the stationary random function $T'_{ij}(\boldsymbol{y}, \tau)$, i.e.

$$\hat{R}_{ij,kl}(\boldsymbol{y}, \boldsymbol{\eta}, \omega) = \int_{\tau_0=-\infty}^{+\infty} \overline{T'_{ij}(\boldsymbol{y}, \tau) T'_{kl}(\boldsymbol{y}+\boldsymbol{\eta}, \tau+\tau_0)}\, \mathrm{e}^{-\mathrm{i}\omega\tau_0}\, \mathrm{d}\tau_0. \tag{2.18}$$

The overbar operation is performed on the non-deterministic part of the integrand in (2.18). The auto-covariance, $\overline{T'_{ij}(\boldsymbol{y}, \tau) T'_{kl}(\boldsymbol{y}+\boldsymbol{\eta}, \tau+\tau_0)}$, depends only upon the time delay $\tau_0$ between the two space–time points we are correlating in $(\boldsymbol{y}, \tau)$ since $T'_{ij}$ is a stationary random function. Notice also that $R_{ij,kl}(\boldsymbol{y}, \boldsymbol{\eta}, \tau_0)$ has a convergent Fourier transform since $\overline{T'_{ij}} = 0$. We can see this immediately if we substitute the definition $T'_{ij} = -\bar{\rho}(\widetilde{v''_i v''_j - v''_i v''_j})$ into the Fourier integral written above,

$$\begin{aligned}\hat{R}_{ij,kl}(\boldsymbol{y}, \boldsymbol{\eta}, \omega) = {} & \bar{\rho}^2(\boldsymbol{y}) \int_{\tau_0=-\infty}^{+\infty} \overline{v''_i v''_j(\boldsymbol{y}, \tau) v''_k v''_l(\boldsymbol{y}+\boldsymbol{\eta}, \tau+\tau_0)}\ \mathrm{e}^{-\mathrm{i}\omega\tau_0}\, \mathrm{d}\tau_0 \\ & - \bar{\rho}^2(\boldsymbol{y}) \int_{\tau_0=-\infty}^{+\infty} \overline{[v''_i v''_j(\boldsymbol{y}, \tau)][v''_k v''_l(\boldsymbol{y}+\boldsymbol{\eta}, \tau+\tau_0)]}\, \mathrm{e}^{-\mathrm{i}\omega\tau_0}\, \mathrm{d}\tau_0. \end{aligned} \tag{2.19}$$

The second term on the right-hand side of (2.19) ensures that the integrand remains bounded so that $R_{ij,kl}(\boldsymbol{y}, \boldsymbol{\eta}, \tau_0) \to 0$ as $\tau_0 \to \pm\infty$ (Batchelor 1953, p. 21).

2.4.1. *Integration in* $\boldsymbol{\eta}$

If we now suppose the variation of each component of the tensor $\hat{I}^{sym}_{kl}$ is small over the lengths $\eta_2$ and $\eta_3$, in comparison to the length that remains correlated, we can introduce an approximation that is equivalent to neglecting the transverse variations in retarded time, and that the Green's function is based upon a parallel shear layer. Hence, following the theoretical argument in Tam & Auriault (1999), we can write $\hat{I}^{sym}_{kl}$ as $\hat{I}^{sym}_{kl}(\boldsymbol{y}+\boldsymbol{\eta}, \omega \,|\, \boldsymbol{x}) \approx \hat{I}^{sym}_{kl}(\boldsymbol{y}, \omega \,|\, \boldsymbol{x})\, \mathrm{e}^{\mathrm{i}k_\infty \eta_1 \cos\theta}$; where the observation point is positioned at an angle $\theta$ to the jet axis and $k_\infty = \omega/c_\infty$ is the wavenumber in the far field. If we substitute this approximation into (2.17), the power spectral density simplifies to

$$\hat{P}(\boldsymbol{x}, \omega) = \int_{V_\infty(\boldsymbol{y})} \hat{I}^{sym}_{ijkl}(\boldsymbol{y}, \omega \,|\, \boldsymbol{x}) \hat{R}^{total}_{ij,kl}(\boldsymbol{y}, \omega)\, \mathrm{d}^3\boldsymbol{y}. \tag{2.20}$$

The wave propagation tensor $\hat{I}^{sym}_{ijkl}$ is now defined as

$$\hat{I}^{sym}_{ijkl}(\boldsymbol{y}, \omega \,|\, \boldsymbol{x}) = \hat{I}^{sym}_{ij}(\boldsymbol{y}, \omega \,|\, \boldsymbol{x}) \hat{I}^{sym}_{kl}(\boldsymbol{y}, -\omega \,|\, \boldsymbol{x}) \tag{2.21}$$

and the integral of $\hat{R}_{ij,kl}(\boldsymbol{y}, \boldsymbol{\eta}, \omega)$ over the vector separation, $\boldsymbol{\eta}$, is

$$\hat{R}^{total}_{ij,kl}(\boldsymbol{y}, \omega) = \int_{\boldsymbol{\eta}} \hat{R}_{ij,kl}(\boldsymbol{y}, \boldsymbol{\eta}, \omega)\, \mathrm{e}^{\mathrm{i}k_\infty \eta_1 \cos\theta}\, \mathrm{d}^3\boldsymbol{\eta}. \tag{2.22}$$

The rest of this paper is devoted to analysing (2.20) for a mean flow based upon a parallel shear layer. We adopt a cylindrically based coordinate system for a jet flow that is circular cylindrical. The fluid properties are then described with respect to the directions $(1, r, \psi)$ so that $\boldsymbol{y} = (y_1, r, \psi)$ and $\boldsymbol{x} = (x_1, R, \Psi)$. For a parallel shear flow, the mean flow is directed axially in $y_1$, and is a function of $r$; and the observer is in the far field at an angle $\theta$ to the jet axis. To evaluate the components of the wave propagation tensor, $\hat{I}^{sym}_{ijkl}$ (using (2.16) and (2.21)), we require a Green's function solution for a parallel flow. That problem is relatively straightforward; for example, the method used by Afsar (2009) is quite convenient for a CFD-based mean

flow, and is used in this paper (see Appendix A). For the Reynolds stress auto-covariance tensor, on the other hand, we model its kinematic properties and define any component we need using a RANS solution of the Stromberg jet, which we obtain from Wu *et al.* (2005) and J. J. McGuirk (private communication). We use isotropy as a paradigm for the kinematics of the turbulence, which, in this paper, we interpret in two ways. First, in the instantaneous sense, we model the stationary random function $T'_{ij}(\boldsymbol{y}, \tau)$. Second, we consider the statistical field, where we have already averaged over time, and model, therefore, the statistical function $R^{total}_{ij,kl}(\boldsymbol{y}, \tau_0)$. In both cases, we calculate the OASPL and compare it with the experiment of Stromberg *et al.* (1980).

## 3. Isotropy in $T'_{ij}(\boldsymbol{y}, \tau)$

### 3.1. *Definition and power spectrum formula*

If we suppose the stationary random function $T'_{ij}(\boldsymbol{y}, \tau)$ is isotropic at any point in $\boldsymbol{y}$, and at any time $\tau$, then

$$T'_{ij}(\boldsymbol{y}, \tau) = \delta_{ij} Q_1(\boldsymbol{y}, \tau). \tag{3.1}$$

Since $T'_{ij}$ is a Cartesian tensor, isotropy implies that $T'_{ij}(\boldsymbol{y}, \tau)$ is completely specified by the scalar field $Q_1(\boldsymbol{y}, \tau)$, such that $Q_1 = T'_{11} = T'_{22} = T'_{33}$ and all off-diagonal components of $T'_{ij}$ are identically zero; i.e. $T'_{12} = T'_{13} = T'_{23} = 0$. A model like this was used by Morris & Farrasat (2002) and implicitly in the work of Goldstein & Leib (2005). The Fourier transform of the Reynolds stress auto-covariance tensor, $\hat{R}_{ij,kl}(\boldsymbol{y}, \boldsymbol{\eta}, \omega)$, can be found by substituting (3.1) into (2.18):

$$\hat{R}_{ij,kl}(\boldsymbol{y}, \boldsymbol{\eta}, \omega) = \delta_{ij}\delta_{kl} \int_{\tau_0=-\infty}^{+\infty} R_{11,11}(\boldsymbol{y}, \boldsymbol{\eta}, \tau_0) \mathrm{e}^{-\mathrm{i}\omega\tau_0} \, \mathrm{d}\tau_0 \; = \; \delta_{ij}\delta_{kl} \hat{R}_{11,11}(\boldsymbol{y}, \boldsymbol{\eta}, \omega). \tag{3.2}$$

Substituting (3.2) into the power spectral density formula, (2.20) gives

$$\hat{P}(\boldsymbol{x}, \omega) = \int_{V_\infty(\boldsymbol{y})} \hat{I}^{sym}_{jjkk}(\boldsymbol{y}, \omega \,|\, \boldsymbol{x}) \hat{R}^{total}_{11,11}(\boldsymbol{y}, \omega) \, \mathrm{d}^3\boldsymbol{y}. \tag{3.3}$$

The term $\hat{I}^{sym}_{jjkk}(\boldsymbol{y}, \omega \,|\, \boldsymbol{x})$ is a diagonal quadratic form because it has diagonal symmetry in its tensor suffixes. Notice that if we retained the momentum transfer term only in (2.16), the power spectrum under instantaneous isotropy would be proportional to $|\widehat{\partial G_j/\partial y_j}|^2$ for any type of mean flow. A formula similar to this result appeared in Morris & Farrasat (2002) and Afsar (2008, p. 130). But we have shown that it simply results when one keeps the momentum transfer part of the propagation tensor $\hat{I}^{sym}_{ij}(\boldsymbol{y}, \omega \,|\, \boldsymbol{x})$ under instantaneous isotropy. In fact, the quadratic form $\hat{I}^{sym}_{jjkk}$ can be expressed analytically for a parallel shear flow. In Appendix A.4, we show that the wave equation for a parallel shear flow implies that $\hat{I}^{sym}_{jjkk} \propto |\widehat{\partial G_j/\partial y_j}|^2$, where the constant of proportionality depends on the Mach-number profile and observation angle, through the Doppler factor.

### 3.2. *The function $R_{11,11}(\boldsymbol{y}, \boldsymbol{\eta}, \tau_0)$ and OASPL calculation*

In the rest of this analysis, we suppose $R_{11,11}(\boldsymbol{y}, \boldsymbol{\eta}, \tau_0)$ is proportional to the turbulent kinetic energy and can be represented by a simple Gaussian-like function. The function is scaled on the local values of the turbulent kinetic energy $k$, the rate of energy dissipation $\epsilon$ and the mean velocity in the axial direction $U(\boldsymbol{y})$ and was defined

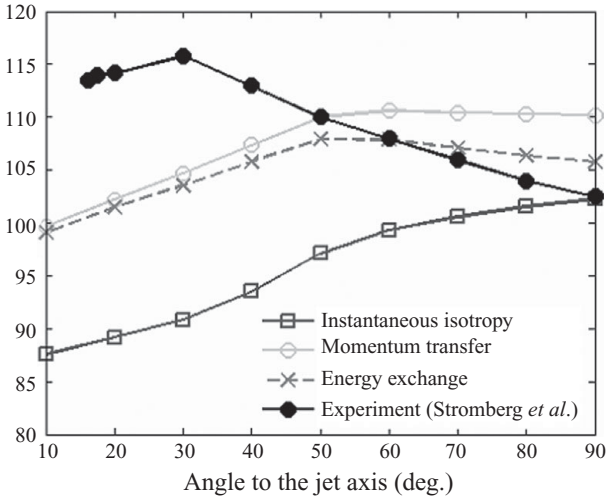


FIGURE 1. Instantaneous isotropy. OASPL (dB) versus observation angle (deg.), where the sound pressure level is $SPL = 10\log(4\pi U_{jet}\hat{P}(\boldsymbol{x},\omega)/p_{ref}^2 D_{jet})$; $D_{jet}$ is the nozzle exit diameter, $U_{jet}$ is the nozzle exit velocity, and $p_{ref}$ is the reference pressure. Observation point is located at $|\boldsymbol{x}| = 30D_{jet}$. The coefficients in (3.3) are $(c_l, c_\tau, A) = (0.5, 1.0, 1.05)$.

by Tam & Auriault (1999). Hence

$$R_{11,11}(\boldsymbol{y},\boldsymbol{\eta},\tau_0) = A^2\bar{\rho}^2(\boldsymbol{y})k^2(\boldsymbol{y})\exp\left(-\frac{|\eta_1|}{U\tau_s(\boldsymbol{y})} - \frac{\ln 2}{l_s^2(\boldsymbol{y})}\left[(\eta_1 - U(\boldsymbol{y})\tau_0)^2 + \eta_2^2 + \eta_3^2\right]\right). \tag{3.4}$$

The quantities $l_s$ and $\tau_s$ describe the characteristic scales of $R_{11,11}(\boldsymbol{y},\boldsymbol{\eta},\tau_0)$; $l_s$ is a length scale and $\tau_s$ represents the time scale at any point $\boldsymbol{y}$. They are defined in the usual way, by the local $k-\epsilon$; i.e. $l_s(\boldsymbol{y}) = c_l(k^{\frac{3}{2}}/\epsilon)(\boldsymbol{y})$ and $\tau_s(\boldsymbol{y}) = c_\tau(k/\epsilon)(\boldsymbol{y})$. The constants $(c_l, c_\tau, A)$ are chosen by trial and error so that the calculated OASPL at 30° and 90° are close enough to the experimental data. To use this function in the power spectral density formula, however, we have to first take the Fourier transform, and then integrate in $\boldsymbol{\eta}$. Those steps are quite straightforward, and can be found in Tam & Auriault (1999). If we use their results, we get

$$\hat{R}_{11,11}^{total}(\boldsymbol{y},\omega) = \int_{\boldsymbol{\eta}} \hat{R}_{11,11}(\boldsymbol{y},\boldsymbol{\eta},\omega)\,\mathrm{e}^{\mathrm{i}k_\infty\eta_1\cos\theta}\,\mathrm{d}^3\boldsymbol{\eta} = 2\left(\frac{\pi}{\ln 2}\right)^{3/2}$$
$$\times A^2\bar{\rho}^2k^2l_s^3\tau_s(\boldsymbol{y})\exp\left(-\frac{\omega^2 l_s^2}{4U^2\ln 2}(\boldsymbol{y})\right)\frac{1}{1+\omega^2\tau_s^2(\boldsymbol{y})\left(1-\frac{U}{c_\infty}(\boldsymbol{y})\cos\theta\right)^2}. \tag{3.5}$$

$\hat{R}_{11,11}^{total}(\boldsymbol{y},\omega)$ is defined using a $k-\epsilon$ RANS calculation of the Stromberg jet. The Green's function is based on the RANS mean flow at $6D_{jet}$ (jet diameters) downstream of the nozzle exit, which is the axial location where the turbulent kinetic energy from the RANS solution is maximum. Even though the wave propagation is based upon a single mean flow, this type of calculation is a useful way to understand the asymptotic properties of the peak jet noise, and one of the calculations we can now, of course, do is to analyse the noise due to momentum transfer and energy exchange separately and in combination. Convergence studies are given in Appendix A.5. In figure 1, we show

the calculated OASPL. Momentum transfer forms the biggest part of the spectrum at large observation angles. However, the cancellation between momentum transfer and energy exchange terms means the calculated OASPL is significantly underpredicted at small observation angles.

## 4. Isotropy in $R^{total}_{ij,kl}(\boldsymbol{y}, \tau_0)$

$T'_{ij}(\boldsymbol{y}, \tau)$ is a stationary random function, which means its integrated auto-covariance, $R^{total}_{ij,kl}$, is statistically stationary, and depends upon $(\boldsymbol{y}, \tau_0)$. So, the next step we take is to model the tensor $R^{total}_{ij,kl}(\boldsymbol{y}, \tau_0)$.

### 4.1. *Definition and power spectrum formula*

For a given time delay $\tau_0$, if we suppose the Cartesian tensor $R^{total}_{ij,kl}$ is isotropic at any point in space $\boldsymbol{y}$, it can only depend upon unity tensors in all possible combinations of their suffixes $(i, j, k, l)$. Hence, $R^{total}_{ij,kl} = \delta_{ij}\delta_{kl}F_1 + \delta_{ik}\delta_{jl}F_2 + \delta_{il}\delta_{jk}F_3$, where $F_{1,\ldots,3}$ are scalar functions each with argument $(\boldsymbol{y}, \tau_0)$. However, the symmetries in the components of tensor $R^{total}_{ij,kl}(\boldsymbol{y}, \tau_0)$ mean that $R^{total}_{ij,kl} = R^{total}_{ji,kl}$ and $R^{total}_{ij,kl} = R^{total}_{ij,lk}$. So $F_2 = F_3$, and $R^{total}_{ij,kl} = \delta_{ij}\delta_{kl}F_1 + (\delta_{ik}\delta_{jl} + \delta_{il}\delta_{jk})F_2$. Now we take the pragmatic step of allowing $F_1 = F_2 = F$ (say) so that the final expression does not depend too much on the individual components of the tensor, and we call this particular form of $R^{total}_{ij,kl}$ statistical isotropy:

$$R^{total}_{ij,kl}(\boldsymbol{y}, \tau_0) = (\delta_{ij}\delta_{kl} + \delta_{ik}\delta_{jl} + \delta_{il}\delta_{jk})F(\boldsymbol{y}, \tau_0). \tag{4.1}$$

In this case, $F(\boldsymbol{y}, \tau_0) = \frac{1}{3}R^{total}_{11,11}(\boldsymbol{y}, \tau_0)$. Alternatively, we could have defined the scalar function using other components from the tensor, because (4.1) implies $R^{total}_{11,11} = R^{total}_{22,22} = R^{total}_{33,33} = 3R^{total}_{11,22} = 3R^{total}_{22,33} = 3R^{total}_{11,33}$, etc. The Fourier transform of $R^{total}_{ij,kl}(\boldsymbol{y}, \tau_0)$ under statistical isotropy is

$$\hat{R}^{total}_{ij,kl}(\boldsymbol{y}, \omega) = (\delta_{ij}\delta_{kl} + \delta_{ik}\delta_{jl} + \delta_{il}\delta_{jk})\frac{1}{3}\int_{\tau_0=-\infty}^{+\infty} R^{total}_{11,11}(\boldsymbol{y}, \tau_0)\,\mathrm{e}^{-\mathrm{i}\omega\tau_0}\,\mathrm{d}\tau_0. \tag{4.2}$$

Substituting (4.2) into the power spectral density formula (2.20) gives

$$\hat{P}(\boldsymbol{x}, \omega) = \frac{1}{3}\int_{V_\infty(\mathbf{y})} \left[\hat{I}^{sym}_{jjkk} + 2\hat{I}^{sym}_{jkjk}\right](\boldsymbol{y}, \omega \,|\, \boldsymbol{x})\hat{R}^{total}_{11,11}(\boldsymbol{y}, \omega)\,\mathrm{d}^3\boldsymbol{y}. \tag{4.3}$$

The quadratic forms ($\hat{I}^{sym}_{jjkk}$ and $\hat{I}^{sym}_{jkjk}$) can easily be found using the wave propagation formulas ((2.16) and (2.21)). Notice that the first term in the integrand of (4.3), $\hat{I}^{sym}_{jjkk}$, is the same diagonal quadratic form that appears under instantaneous isotropy (see (3.3)); under statistical isotropy, however, we have admitted the quadratic form $\hat{I}^{sym}_{jkjk}$ into the integrand of the power spectrum. Both of these quadratic forms are real and positive-definite; for example, we show in Appendix A.4, that $\hat{I}^{sym}_{jjkk}$ can be expressed analytically to show it is actually proportional to $|\widehat{\partial G_j/\partial y_j}|^2$. On the other hand, the second quadratic form in (4.3) has Hermitian symmetry in the tensor suffixes, since $\hat{I}^{sym}_{jkjk} = \hat{I}^{sym}_{kjkj} = \hat{I}^{sym}_{jkkj}$ and $\hat{I}^{sym}_{jkjk}(\boldsymbol{y}, \omega \,|\, \boldsymbol{x}) = \hat{I}^{sym}_{jk}(\boldsymbol{y}, \omega \,|\, \boldsymbol{x})\hat{I}^{sym}_{jk}(\boldsymbol{y}, -\omega \,|\, \boldsymbol{x}) = |\,\hat{I}^{sym}_{jk}|^2$. The Hermitian quadratic form will make the biggest contribution to the value of the integral in (4.3) since it involves both the diagonal and off-diagonal terms in the second-rank wave propagation tensor $\hat{I}^{sym}_{jk}$.

### 4.2. *Calculation of the OASPL*

The function $R_{11,11}$ is given by (3.4), and the wave propagation terms (the quadratic forms) are based upon a mean flow at $6D_{jet}$ downstream of the nozzle exit. In

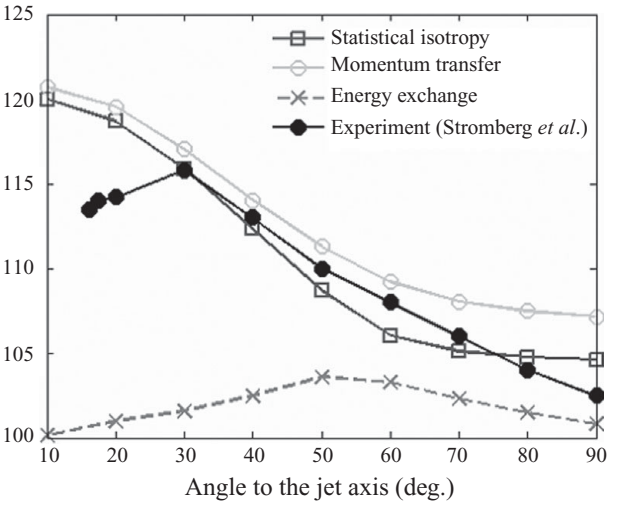


FIGURE 2. Statistical isotropy. OASPL (dB) versus observation angle (deg.), where the sound pressure level is $SPL = 10\log(4\pi U_{jet}\hat{P}(\boldsymbol{x},\omega)/p_{ref}^2 D_{jet})$; $D_{jet}$ is the nozzle exit diameter, $U_{jet}$ is the nozzle exit velocity, and $p_{ref}$ is the reference pressure. Observation point is located at $|\boldsymbol{x}| = 30D_{jet}$. The coefficients in (4.3) are $(c_l, c_\tau, A) = (0.5, 1.0, 0.735)$.

Appendix A.5, we show the numerical calculation of the quadratic forms is converged and robust. In figure 3, we assess the contribution momentum transfer and energy exchanges play to the OASPL. If we consider the behaviour between 30° and 90°, the calculation manages to capture the correct OASPL at 30°, although at larger angles the predictions deviate from experiment by about 2 dB. But what is important to realize here is that, on a purely diagnostic basis, (4.3) is able to follow the correct trend of the OASPL curve at least between 30° and 90°. Remember, there are difficulties in measuring the OASPL at small angles, less than 30° (Morris 2009). Figure 3 also shows that momentum transfer forms the biggest part of the spectrum at small observation angles, less than the critical angle that defines the 'zone of silence' of the pressure-like Green's function $\hat{G}_4$. The noise due to energy exchanges is important too, for example, the cancellation between the momentum transfer terms and the energy exchange terms in (2.16) means that the total value of the integral (4.3) is lower than if momentum transfer is taken alone. Indeed, the cancellation introduced by the energy exchange contribution, within certain components of $\hat{I}_{jk}^{sym}$ that reduce the magnitude of the positive-definite quadratic forms, is greatest at larger angles, near 90°.

## 5. Low-frequency properties

By supposing $R_{ij,kl}^{total}(\boldsymbol{y},\tau_0)$, the integrated Reynolds stress auto-covariance tensor, is isotropic in all of its tensor suffixes in the particular manner of (4.1), the calculated OASPL is in reasonable agreement with experiment between 30° and 90°. At 30°, the calculation is accurate, and as we approach 90°, there is a deviation of about 2 dB. For angles less than 30°, the observed OASPL decreases (see Morris 2009, for an explanation) but the calculation continues to show an increase in overall sound pressure (figure 2). The reason why this occurs can be understood mathematically.

Under statistical isotropy, we introduced two quadratic forms into the integrand of the power spectral density formula, $\hat{I}_{jjkk}^{sym}(\boldsymbol{y},\omega\,|\,\boldsymbol{x})$, and the Hermitian quadratic form

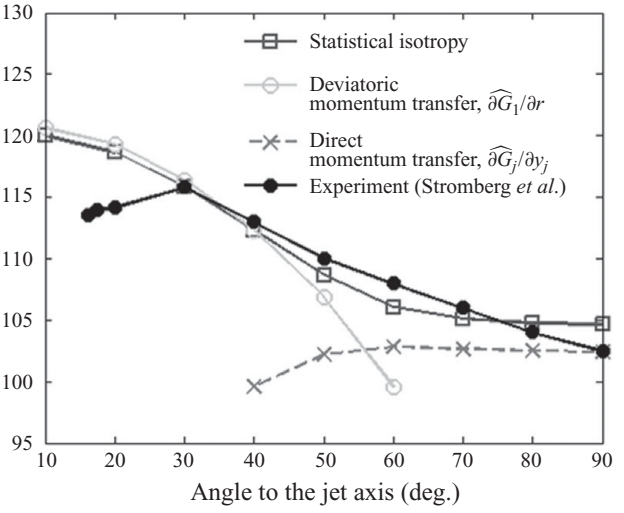


FIGURE 3. Dominant terms under statistical isotropy. Same as figure 2.

$\hat{I}^{sym}_{jkjk}(\boldsymbol{y}, \omega \,|\, \boldsymbol{x})$ (given by 4.3). Our numerical calculations have shown that statistical isotropy can describe the behaviour of the OASPL curve between 30° and 90° to an accuracy of about 2 dB, as we summarize in figure 3. The diagonal quadratic form $\hat{I}^{sym}_{jjkk}$, by definition, involves the diagonal elements of the second-rank wave propagation tensor $\hat{I}^{sym}_{jk}$ only, and as we prove in Appendix A.4, it remains proportional to $|\widehat{\partial G_j}/\partial y_j|^2$ for any value in $(\boldsymbol{y}, \omega \,|\, \boldsymbol{x})$. The Hermitian quadratic form, $\hat{I}^{sym}_{jkjk}$, on the other hand, includes all of the terms from $\hat{I}^{sym}_{jk}$ (diagonal and off-diagonal). Numerical calculations show that the peak overall sound pressure, at small angles to jet axis, is due to the presence of the off-diagonal term, $\widehat{\partial G_1}/\partial r$, in $\hat{I}^{sym}_{jkjk}$, whereas at larger observation angles, the trace term $\widehat{\partial G_j}/\partial y_j$ in the diagonal quadratic form $\hat{I}^{sym}_{jjkk}$ starts to dominate the total value of the power spectral density integral (see figure 3).

The directional properties of these dominant terms ($\widehat{\partial G_1}/\partial r$ and $\widehat{\partial G_j}/\partial y_j$) in the quadratic forms can be easily understood using their explicit form given by (A 10) in Appendix A, in the low-frequency limit. We show in Appendix B that the convective derivative of the pressure-like Green's function, $\widehat{D_1 G_4}/D\tau$, will remain $O(\omega^2)$ as $\omega \to 0$ (in our notation, $\widehat{D_1}/D\tau = \mathrm{i}\omega(1 + M(r)\cos\theta)$ and $M(r) = U(r)/c_\infty$, where $U(r)$ is the mean velocity in the axial direction). This result can also be inferred from the work of Goldstein (1975) and Balsa (1977), who considered the low-frequency acoustic radiation problem, but for point sources in motion. Hence, if we make use of this result, and use the expression for the components of the tensor in Appendix A (A 10), we find the following.

(*a*) *Deviatoric momentum transfer: off-diagonal term in momentum transfer tensor*

$$\begin{aligned}\frac{\widehat{\partial G_1}}{\partial r}(\boldsymbol{y}, \omega \,|\, \boldsymbol{x}) &\propto \frac{1}{(1 - M(r)\cos\theta)^2}\frac{\cos\theta}{k_\infty}\left[\frac{\partial}{\partial r} - \frac{2\cos\theta}{(1 - M(r)\cos\theta)}\frac{\mathrm{d}M}{\mathrm{d}r}(r)\right]\frac{\widehat{D_1 G_4}}{D\tau}(\boldsymbol{y}, \omega \,|\, \boldsymbol{x}) \\ &\sim \frac{\omega\cos^2\theta}{(1 - M(r)\cos\theta)^3}\frac{\mathrm{d}U}{\mathrm{d}r}(r) \quad (\because \widehat{D_1 G_4}/D\tau = O(\omega^2) \quad \lim\omega \to 0). \\ &\therefore \widehat{\partial G_1}/\partial r = O(\omega) \quad (\lim\omega \to 0). \end{aligned} \tag{5.1}$$

(*b*) *Direct momentum transfer: diagonal terms in momentum transfer tensor*

$$\frac{\widehat{\partial G_j}}{\partial y_j}(\boldsymbol{y},\omega\,|\,\boldsymbol{x}) \propto \frac{\widehat{D_1 G_4}}{D\tau}(\boldsymbol{y},\omega\,|\,\boldsymbol{x}).$$

$$\therefore\ \widehat{\partial G_j}/\partial y_j = O(\omega^2) \quad (\lim \omega \to 0). \tag{5.2}$$

The term $\widehat{\partial G_1}/\partial r$ is asymptotically bigger than $\widehat{\partial G_j}/\partial y_j$ in the limit of very low frequency. As $\omega \to 0$, $\widehat{\partial G_j}/\partial y_j = O(\omega^2)$, whereas $\widehat{\partial G_1}/\partial r = O(\omega)$. This happens because in (5.1), the radial derivative of $\widehat{D_1 G_4}/D\tau$, the term $\partial/\partial r(\widehat{D_1 G_4}/D\tau)$, will always be asymptotically smaller than $\widehat{D_1 G_4}/D\tau$ itself as $\omega \to 0$ (see Appendix B). Therefore, in the first line of (5.1), the second term in the square brackets, proportional to $\widehat{D_1 G_4}/D\tau$, is always the asymptotically dominant term at very low frequencies.

### 5.1. *Isotropy as a paradigm–interpretation*

The results in this paper suggest that, firstly, isotropy in $R^{total}_{ij,kl}(\boldsymbol{y},\tau_0)$ does not imply that the stationary random function $T'_{ij}$ is itself isotropic. Allowing $T'_{ij}(\boldsymbol{y},\tau)$ to be isotropic is isotropy in the instantaneous sense, and this can only admit the diagonal quadratic form $\hat{I}^{sym}_{jjkk}$ into the integrand of the power spectrum formula (3.3). And as we proved in Appendix A.4, the diagonal quadratic form remains proportional to $|\widehat{\partial G_j}/\partial y_j|^2$ for any value in $(\boldsymbol{y},\omega\,|\,\boldsymbol{x})$; i.e. $\hat{I}^{sym}_{jjkk} \propto |\widehat{\partial G_j}/\partial y_j|^2$. So, by allowing $T'_{ij}$ to be isotropic in the instantaneous sense, it actually implies the sound power will always remain $O(\omega^4)$ as $\omega \to 0$. On the other hand, if one supposes the integrated auto-covariance of $T'_{ij}$, the rank four tensor $R^{total}_{ij,kl}(\boldsymbol{y},\tau_0)$ is isotropic in all of its tensor suffixes, we admit two terms in the power spectrum formula: $\hat{I}^{sym}_{jjkk}$, and the Hermitian form $\hat{I}^{sym}_{jkjk}$. As $\omega \to 0$, the acoustic spectrum is now proportional to the mean-flow-dependent quantity $\omega^2(\mathrm{d}U/\mathrm{d}r)^2$, where $\mathrm{d}U(r)/\mathrm{d}r$ is the gradient of the mean velocity in the axial direction. This is because when the frequency is very low, any term in the noise spectrum that is multiplied by $\omega^2(\mathrm{d}U/\mathrm{d}r)^2$ (5.1) will dominate over one that is multiplied by $\omega^4$ (5.2). As Goldstein (1975) remarked in his article, 'the velocity gradient acts like a sounding board to increase the efficiency of the quadrupole radiation (to that of a dipole).'

The directivity of this shear term $\widehat{\partial G_1}/\partial r$ is highest at small angles to the jet axis because its sound pressure scales as $\cos^4\theta/(1-M(r)\cos\theta)^6$. This behaviour is different from Goldstein (1975) because he considered multipole sources in motion at a convection Mach number of $\mathscr{M}_c$, but this particular type of directivity that we have shown can be recovered from the results in Goldstein (1975) by setting $\mathscr{M}_c = 0$. However, because of this pre-factor, $\cos^4\theta$, in the directivity, the OASPL will continue to increase as $\theta \to 0$, when $\hat{I}^{sym}_{jkjk}$ is defined by a Green's function based upon a single mean flow, which is contrary to what the experiments show. But as we pointed out earlier, it is important to realize here that, on a purely theoretical basis, (4.3) is able to follow the correct trend of the OASPL curve between 30° and 90°. Moreover, as we explained, isotropy in $R^{total}_{ij,kl}(\boldsymbol{y},\tau_0)$ (4.1) naturally recovers this behaviour. In the spirit of Lilley (1958), at small angles to the jet axis, the overall sound pressure closely matches the Hermitian quadratic form $\hat{I}^{sym}_{jkjk}$ (or the 'shear-noise'-type term), whereas at larger observation angles the diagonal quadratic form $\hat{I}^{sym}_{jjkk}$ (or the 'self-noise'-type term) starts to dominate the total value of the power spectral density integral.

### 5.2. *Sensitivity of the calculated OASPL to* $R_{11,11}$

Our analysis in this paper has shown that explicit self-noise ($\hat{I}^{sym}_{jjkk}$) and shear noise ($\hat{I}^{sym}_{jkjk}$) terms can be recovered in the power spectrum if $R^{total}_{ij,kl}(\boldsymbol{y},\tau_0)$ is taken to be

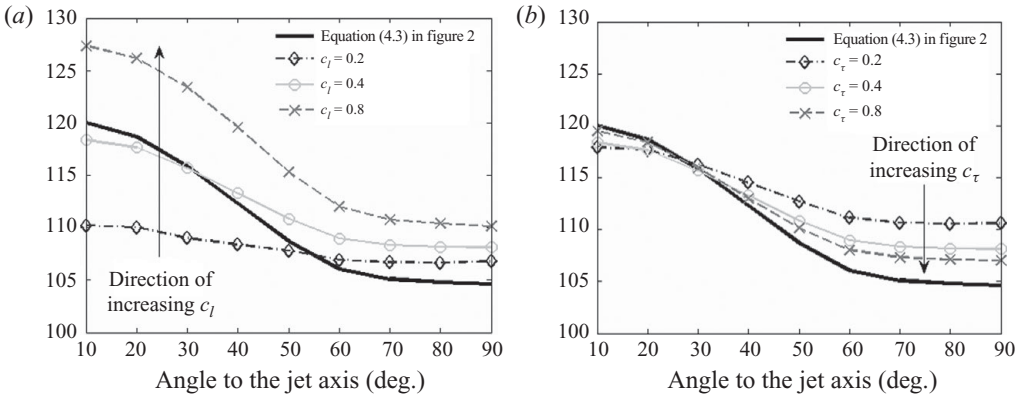


FIGURE 4. Sensitivity of the OASPL (dB) to $R_{11,11}$. Same as figure 2. The amplitude constant is the same as figure 2, $A = 0.735$. (*a*) $c_\tau = 0.4$ (*b*) $c_l = 0.4$.

isotropic in all of its tensor suffixes. However, the power spectral density formula in (4.3) required one to tune the empirical constants $(c_l, c_\tau, A)$ in the formula for $R_{11,11}$ (defined by (3.4)). Although this tuning process poses no particular difficulty, it is important to assess how sensitive the calculated peak sound is to the variation of $(c_l, c_\tau, A)$. The way we show this is to vary $(c_l, c_\tau)$ for the same value of the amplitude constant $A$ that we used in figure 2. In figure 4, we compute the sound pressure under statistical isotropy (4.3) by first varying $c_l$ and keeping $c_\tau = 0.4$ fixed (figure 4*a*) and then varying $c_\tau$ and keeping $c_l = 0.4$ fixed (figure 4*b*). In both figures, the Green's functions and wave propagation terms are calculated using the mean flow at $6D_{jet}$ downstream of the nozzle exit. Even though the $\widehat{\partial G_1/\partial r}$ term makes the Hermitian quadratic form $\hat{I}^{sym}_{jkjk}$ dominant at small observation angles, the actual shape of the OASPL curve depends on $R_{11,11}$ as well.

### 5.3. *Departure from statistical isotropy and non-parallel mean flow effects*

Under statistical isotropy, we required one component of the Reynolds stress auto-covariance tensor (4.1). In reality, of course, $R_{ij,kl}(\boldsymbol{y}, \boldsymbol{\eta}, \tau_0)$ possesses 36 independent components and all of these terms contribute to the acoustic spectrum. It would be difficult, however, to obtain the space–time history of each component in order to do such a complete calculation. Hence, a more realistic kinematic model of the turbulence is the next logical step. In some recent work, an axisymmetric model of the Reynolds stress auto-covariance was developed by Afsar (2010) by introducing two approximations. First, that the tensor depends upon the transverse vector separation only through its magnitude, and second that this approximate Reynolds stress auto-covariance tensor is itself axisymmetric. Afsar (2010) referred to these two approximations, when taken together, as the statistical axisymmetry model. Equation (5.6) in Afsar (2010) shows that under statistical axisymmetry, the acoustic spectrum in cold jet flows is given by the sum of two groups of terms. For a parallel mean flow Green's function in the low-frequency limit, one of these groups possesses a wave propagation term that is similar in behaviour to the Hermitian quadratic form $\hat{I}^{sym}_{jkjk}$; i.e. the term increases in magnitude with six inverse Doppler factors as the observation angle is reduced, and is zero at 90°.

Non-parallel flow effects are expected to play an important role in low-frequency sound, particularly at small observation angles to the jet axis (see Karabasov *et al.* 2010, figure 13*a*). The numerical computations of the adjoint equations (2.10)–(2.12)

in Karabasov *et al.* (2010) show that non-parallelism in the mean flow model can lead to a reduction in the low-frequency sound below that predicted by the parallel flow model given by (5.1). However, the present low-frequency asymptotic analysis for a parallel flow (described in detail in Appendix B) will provide a coherent starting point to develop a similar asymptotic theory in non-parallel flows.

## 6. Conclusions

We have re-analysed the jet noise problem to explicitly show the existence of 'self-noise' and 'shear-noise'-type terms that were first envisaged by Lilley (1958). We set up the problem as an acoustic analogy using the hyperbolic conservation form of the Euler equations derived by Goldstein (2002). We showed that by supposing that the integrated auto-covariance tensor ($R^{total}_{ij,kl}$) of the Reynolds-stress-source term ($T'_{ij}$) is isotropic in all of its tensor suffixes, it introduces two terms into the power spectral density formula that can be naturally identified as the self-noise and shear noise in the spirit of Lilley. This is because one of these terms is biggest at large observation angles (self-noise-type term, (5.2)), while the other is dominant at small angles (shear-noise-type term, (5.1)) and is proportional to $\omega^2(\mathrm{d}U/\mathrm{d}r)^2$ (where $\mathrm{d}U/\mathrm{d}r$ is the local mean flow gradient). In terms of its directional properties, this shear term is proportional to $\cos^4\theta/(1-M(r)\cos\theta)^6$ (where $M(r)=U(r)/c_\infty$ is the local Mach-number profile and $\theta$ is the observation angle with respect to the jet axis) and was first shown to exist by Goldstein (1975), and indeed it was more recently confirmed by Goldstein & Leib (2008) who found identical properties, as we have shown in this paper. Our analysis also proves that this shear term will not occur if the instantaneous strength of $T'_{ij}$ is taken to be isotropic itself. Moreover, we have shown that the sound pressure of this shear term is crucially dependent on the functional properties defining the correlation function of the turbulence, because the correlation function multiplies both terms in the integrand of the power spectral density formula.

This work was conducted when the author was a graduate student at the Engineering Department at Cambridge University. It was part of a collaborative project on jet noise funded by the Engineering and Physical Sciences Research Council (EPSRC) and their support is gratefully acknowledged. The author is grateful for helpful discussions with colleagues at the Universities of Cambridge and Loughborough, and Rolls-Royce, particularly Professor A. Dowling and also Professor J. McGuirk, Drs S. Karabasov, T. Hynes, G. Page and Dr J. Wu who provided the CFD data. The paper was written when the author was visiting the NASA Glenn Research Center as part of the David Crighton Fellowship awarded to him by the Department of Applied Mathematics and Theoretical Physics, Cambridge. The author would like to thank Dr S. J. Leib of the Ohio Aerospace Institute for helpful comments and suggestions.

## Appendix A. Green's function

### A.1. *Solution for pressure-like Green's function*

In this Appendix, we briefly go through the evaluation of each component of the second-rank wave propagation tensor $\hat{I}_{ij}(\boldsymbol{y},\omega\,|\,\boldsymbol{x})$ for a Green's function defined by a parallel mean flow. The mean flow conditions for a parallel shear layer are given as usual by $\tilde{v}_j(\boldsymbol{y})=\delta_{j1}U(y_2,y_3)$, $\bar{p}(\boldsymbol{y})=p_\infty$, $\tilde{h}(\boldsymbol{y})=\tilde{h}(y_2,y_3)$ and $\bar{\rho}(\boldsymbol{y})=\bar{\rho}(y_2,y_3)$ (Lilley

1974). In this case, the adjoint equations (2.10)–(2.12) reduce to

$$\mathrm{i}\omega\hat{G}_j + U\frac{\partial\hat{G}_j}{\partial y_1} - \hat{G}_1\frac{\partial U}{\partial y_j} + \tilde{h}\frac{\partial\hat{G}_4}{\partial y_j} = 0 \quad j = 1, \ldots, 3, \tag{A 1}$$

$$\frac{\mathrm{i}\omega}{(\gamma-1)}\hat{G}_4 + \frac{U}{(\gamma-1)}\frac{\partial\hat{G}_4}{\partial y_1} + \frac{\partial\hat{G}_j}{\partial y_j} = \delta(\boldsymbol{y}-\boldsymbol{x}). \tag{A 2}$$

The adjoint mass equation takes the simple form, $\hat{\mathrm{D}}_1\hat{G}_0/\mathrm{D}\tau = 0$, where $\hat{\mathrm{D}}_1/\mathrm{D}\tau$ is the convective derivative in the axial direction and is defined by $\hat{\mathrm{D}}_1/\mathrm{D}\tau \equiv [\mathrm{i}\omega + U(y_2, y_3)\partial/\partial y_1]$. This equation implies that $\hat{G}_0$ is convected in the $y_1$ direction and since $\hat{G}_0$ is zero at infinity, it must be zero everywhere, so that $\partial\hat{G}_0/\partial y_i = 0$. Afsar (2009) showed that if we introduce a new Green's function variable, $G_5(\boldsymbol{y}, \tau\,|\,\boldsymbol{x}, t)$, defined by $G_5 = \frac{1}{(\gamma-1)}\frac{\mathrm{D}_1 G_4}{\mathrm{D}\tau}$, then we can rewrite (A 2) in a conservation form, i.e.

$$\frac{1}{\tilde{c}^2}\frac{\hat{\mathrm{D}}_1^2\hat{G}_j}{\mathrm{D}\tau^2} + \frac{\partial\hat{G}_5}{\partial y_j} = 0, \quad j = 1, \ldots, 3, \tag{A 3}$$

$$\hat{G}_5 + \frac{\partial\hat{G}_j}{\partial y_j} = \delta(\boldsymbol{y}-\boldsymbol{x}). \tag{A 4}$$

Since we want to obtain the solution to $\hat{G}_5(\boldsymbol{y}, \omega\,|\,\boldsymbol{x})$ for a jet flow that is circular cylindrical, we express the field variables in terms of a cylindrical polar coordinate system, where $\boldsymbol{y} = (y_1, r, \psi)$ and $\boldsymbol{x} = (x_1, R, \Psi)$. The observation point is at the location $\boldsymbol{x}$, outside the jet flow, at an angle $\theta$ to the jet axis $y_1$.

In the present analysis, we are restricting ourselves to a cold jet flow, where the fluctuations in stagnation enthalpy and density are small compared to the velocity field. Although we did allow $\rho(\boldsymbol{y}, \tau) \approx \bar{\rho}(\boldsymbol{y})$, the variation of $\bar{\rho}(\boldsymbol{y})$ will still be small in comparison to $\tilde{v}_i(\boldsymbol{y})$. For example, we would expect the derivative of $\bar{\rho}(\boldsymbol{y})$ in the transverse direction $\boldsymbol{y}_\perp = (y_2, y_3)$, i.e. the term $\mathrm{d}\bar{\rho}(\boldsymbol{y})/\mathrm{d}\boldsymbol{y}_\perp$, to be small in comparison to the derivative of $U(\boldsymbol{y})$ with respect to $\boldsymbol{y}_\perp$ when suitably non-dimensionalized; i.e. we expect $(1/U_{jet})\,\mathrm{d}U(\boldsymbol{y})/\mathrm{d}\boldsymbol{y}_\perp \gg (1/\rho_\infty)\,\mathrm{d}\bar{\rho}(\boldsymbol{y})/\mathrm{d}\boldsymbol{y}_\perp$. Therefore, we can safely allow $\bar{\rho}(\boldsymbol{y}) \approx \rho_\infty$, and $\tilde{c}^2(\boldsymbol{y}) \approx c_\infty^2$, in the conservation form of the adjoint momentum equation A3. Now if we take Fourier transforms in $y_1$ and $\psi$, we can reduce the conservation equations into two ordinary differential equations for $\widetilde{G}_5(r, k, m, \omega\,|\,\boldsymbol{x})$ and $\widetilde{G}_r(r, k, m, \omega\,|\,\boldsymbol{x})$ that take the form

$$\frac{\mathrm{d}\widetilde{G}_5}{\mathrm{d}r} = k_\infty^2\left(1 + M(r)\frac{k}{k_\infty}\right)^2\widetilde{G}_r, \tag{A 5}$$

$$\frac{\mathrm{d}\widetilde{G}_r}{\mathrm{d}r} = \left[\frac{(k/k_\infty)^2}{\left(1 + M(r)\dfrac{k}{k_\infty}\right)^2} + \frac{(m/r)^2}{k_\infty^2\left(1 + M(r)\dfrac{k}{k_\infty}\right)^2} - 1\right]\widetilde{G}_5 - \frac{\widetilde{G}_r}{r}, \tag{A 6}$$

where $k$ is the axial wavenumber, $m$ is the azimuthal mode, $k_\infty = \omega/c_\infty$ and $M(r) = U(\boldsymbol{y})/c_\infty$.

The key feature of this system of ordinary differential equations is the elimination of the mean flow derivatives – the coefficients in (A 5) and (A 6) are functions of the mean flow only (Afsar 2009). The solution for $\widetilde{G}_5$ and $\widetilde{G}_r$ can be found by numerically integrating (A 5) and (A 6) using the standard variable-step fourth-order Runge–Kutta

scheme, where, following Tam & Auriault (1998), the initial conditions follow easily by realizing that $\widetilde{G}_4$ is bounded algebraically (as $r^m$, where $m$ is the azimuthal mode number) near the axis $r=0$. The solution to $\hat{G}_5(\boldsymbol{y},\omega\,|\,\boldsymbol{x})$ then follows by taking the inverse Fourier transforms in $k$ and $m$. The inverse Fourier transform in azimuthal mode $m$ is performed by expressing the solution as a Fourier series in $m$. Since the solution to $\hat{G}_5(\boldsymbol{y},\omega\,|\,\boldsymbol{x})$ must be weakly causal in order for it to remain bounded in the field space $(\boldsymbol{y},\omega\,|\,\boldsymbol{x})$, and since we want the solution when the field point $\boldsymbol{x}$ is in the far field (and $|\,\boldsymbol{x}\,|\to\infty$), we can evaluate the inverse Fourier transform in $k$ using the method of stationary phase. Because we are allowing $|\,\boldsymbol{x}\,|\to\infty$, we neglect any residue contribution that arises when we deform the contour of integration from the real $k$-axis to the path of steepest descent. Moreover, for the same reason, we neglect the residue contribution from any poles in the integrand (in the complex $k$-plane) that are crossed as the contour is deformed and any branch cut contributions that may also arise. Then, the leading-order solution to $\hat{G}_5(\boldsymbol{y},\omega\,|\,\boldsymbol{x})$ at the stationary phase point $k=-k_\infty\cos\theta$, is given by

$$\hat{G}_5(\boldsymbol{y},\omega\,|\,\boldsymbol{x})=-\frac{k_\infty^2(1-M(r)\cos\theta)}{4\pi\,|\,\boldsymbol{x}\,|}\,\mathrm{e}^{-\mathrm{i}k_\infty\{y_1\cos\theta-|\,\boldsymbol{x}\,|\}}\times\sum_{m=0}^{+\infty}(-\mathrm{i})^m\epsilon_m A_m(\omega,\theta)\widetilde{G}_5(r)\cos m(\psi-\Psi),\quad(\mathrm{A}\,7)$$

where $\epsilon=1$ if $m=0$, and $\epsilon=2$ if $m\geqslant 1$, for integral $m\geqslant 1$. But at large values of $r$ outside the jet flow in the outer region, the mean flow is zero, and $\hat{G}_5(\boldsymbol{y},\omega\,|\,\boldsymbol{x})$ must satisfy the usual (homogeneous field) wave equation there. The solution of $\hat{G}_5(\boldsymbol{y},\omega\,|\,\boldsymbol{x})$ in the outer region is then simply the analytical solution due to a point sink, i.e.

$$\hat{G}_5(\boldsymbol{y},\omega\,|\,\boldsymbol{x})=-\frac{k_\infty^2(1-M(r)\cos\theta)}{4\pi\,|\,\boldsymbol{x}\,|}\mathrm{e}^{-\mathrm{i}k_\infty\{y_1\cos\theta-|\,\boldsymbol{x}\,|\}}\cdot\sum_{m=0}^{+\infty}(-\mathrm{i})^m\epsilon_m\big[J_m(k_\infty R_\infty\sin\theta)+B_m(\omega,\theta)H_m^{(1)}(k_\infty R_\infty\sin\theta)\big]\cos m(\psi-\Psi).\quad(\mathrm{A}\,8)$$

The terms $A_m(\omega,\theta)$ and $B_m(\omega,\theta)$ are constants in $r$, and are found by *patching* solution (A 7) to solution (A 8); i.e. by equating their value, and derivative, in the $r$-direction, at a far location. For example, if we patch the solutions together at the point $R_\infty$, by taking $R_\infty=20D_{jet}$, where $D_{jet}$ is the nozzle exit diameter, is quite sufficient. Mathematically, however, at the point $R_\infty$, the numerical solution $\widetilde{G}_5(r)$ is equal to the analytical solution given by (A 8). The robustness of the calculation can be found in Afsar (2009).

### A.2. *Wave propagation tensor*

As we have defined the Green's function $\hat{G}_5(\boldsymbol{y},\omega\,|\,\boldsymbol{x})$, we can determine each component of the wave propagation tensor $\hat{I}_{ij}(\boldsymbol{y},\omega\,|\,\boldsymbol{x})$ (2.16) in a similar way. Indeed, one advantage using the $\hat{G}_5$ variable is that each component of $\hat{I}_{ij}$ can be written in terms of $\hat{G}_5(\boldsymbol{y},\omega\,|\,\boldsymbol{x})$. We use a 'wide hat' symbol to imply that each component of the tensor is evaluated mode-by-mode, and, if a radial derivative is there, we differentiate mode-by-mode; then we add the modes together, remembering the constant $\epsilon_m$ that multiplies the Green's function solution, where $\epsilon=1$ if $m=0$; and $\epsilon=2$ if $m\geqslant 1$ (for all integral values of $m$). Now we can express (2.16) directly in terms of $\hat{G}_5(\boldsymbol{y},\omega\,|\,\boldsymbol{x})$.

Hence,

$$\hat{I}_{ij}(\boldsymbol{y},\omega\,|\,\boldsymbol{x}) = \underbrace{\widehat{\frac{\partial G_j}{\partial y_i}}(\boldsymbol{y},\omega\,|\,\boldsymbol{x})}_{\text{Momentum transfer: term I}} + \underbrace{\frac{\mathrm{i}\delta_{j1}}{k_\infty}\frac{(\gamma-1)}{[1-M(r)\cos\theta]}\frac{\partial M}{\partial y_i}(r)\hat{G}_5(\boldsymbol{y},\omega\,|\,\boldsymbol{x})}_{\text{Energy exchange: term IIa}}$$
$$\underbrace{-\delta_{j1}c_\infty M(r)\widehat{\frac{\partial G_4}{\partial y_i}}(\boldsymbol{y},\omega\,|\,\boldsymbol{x})}_{\text{Energy exchange: term IIb}} + \underbrace{(\gamma-1)\frac{\delta_{ij}}{2}\hat{G}_5(\boldsymbol{y},\omega\,|\,\boldsymbol{x})}_{\text{Energy exchange: term IIIa}}. \tag{A 9}$$

Notice the consistency in notation here; the 'wide hat' only appears on the terms that involve differentiating the Green's function. Energy exchange terms IIa and IIIa are proportional to Green's function, and not its derivative, so the 'hat' appears over $G_5$ only. The tensor is written out in the list of equations below, where each component of the tensor carries the dimensions of $\hat{G}_5$; and, for clarity, we have written the angular derivatives as $\partial/\partial\psi$, but they are to be understood by $\partial/\partial\psi \equiv \mathrm{i}m$:

$$\hat{I}_{11}(\boldsymbol{y},\omega\,|\,\boldsymbol{x}) = \left[\frac{(\gamma-1)}{2}\hat{G}_5 + \frac{(\gamma-1)M(r)\cos\theta}{(1-M(r)\cos\theta)}\hat{G}_5 - \frac{\cos^2\theta}{(1-M(r)\cos\theta)^2}\hat{G}_5\right](\boldsymbol{y},\omega\,|\,\boldsymbol{x}), \tag{A 10a}$$

$$\hat{I}_{r1}(\boldsymbol{y},\omega\,|\,\boldsymbol{x}) = \frac{\mathrm{i}}{k_\infty}\frac{(\gamma-1)\,\mathrm{d}M(r)/\mathrm{d}r}{(1-M(r)\cos\theta)}\hat{G}_5(\boldsymbol{y},\omega\,|\,\boldsymbol{x})$$
$$+\frac{\mathrm{i}}{k_\infty}\frac{(\gamma-1)M(r)}{(1-M(r)\cos\theta)}\left[\widehat{\frac{\partial G_5}{\partial r}} + \frac{\hat{G}_5\,\mathrm{d}M(r)/\mathrm{d}r\cos\theta}{(1-M(r)\cos\theta)}\right](\boldsymbol{y},\omega\,|\,\boldsymbol{x})$$
$$-\frac{\mathrm{i}}{(1-M(r)\cos\theta)^2}\frac{\cos\theta}{k_\infty}\left[\widehat{\frac{\partial G_5}{\partial r}} + \frac{2\hat{G}_5\,\mathrm{d}M(r)/\mathrm{d}r\cos\theta}{(1-M(r)\cos\theta)}\right](\boldsymbol{y},\omega\,|\,\boldsymbol{x}), \tag{A 10b}$$

$$\hat{I}_{\psi 1}(\boldsymbol{y},\omega\,|\,\boldsymbol{x}) = \frac{\mathrm{i}}{k_\infty}\left[\frac{(\gamma-1)M(r)}{(1-M(r)\cos\theta)} - \frac{\mathrm{i}\cos\theta}{(1-M(r)\cos\theta)^2}\right]\frac{1}{r}\widehat{\frac{\partial G_5}{\partial\psi}}(\boldsymbol{y},\omega\,|\,\boldsymbol{x}), \tag{A 10c}$$

$$\hat{I}_{1r}(\boldsymbol{y},\omega\,|\,\boldsymbol{x}) = -\mathrm{i}\frac{\cos\theta}{k_\infty}\frac{1}{(1-M(r)\cos\theta)^2}\widehat{\frac{\partial G_5}{\partial r}}(\boldsymbol{y},\omega\,|\,\boldsymbol{x}), \tag{A 10d}$$

$$\hat{I}_{rr}(\boldsymbol{y},\omega\,|\,\boldsymbol{x}) = \frac{(\gamma-1)}{2}\hat{G}_5(\boldsymbol{y},\omega\,|\,\boldsymbol{x}) + \frac{1}{k_\infty^2(1-M(r)\cos\theta)^2}$$
$$\times\left[\widehat{\frac{\partial^2 G_5}{\partial r^2}} + \frac{2\,\mathrm{d}M(r)/\mathrm{d}r\ \cos\theta}{(1-M(r)\cos\theta)}\widehat{\frac{\partial G_5}{\partial r}}\right](\boldsymbol{y},\omega\,|\,\boldsymbol{x}), \tag{A 10e}$$

$$\hat{I}_{\psi r}(\boldsymbol{y},\omega\,|\,\boldsymbol{x}) = \frac{1}{k_\infty^2(1-M(r)\cos\theta)^2}\left[\frac{1}{r}\widehat{\frac{\partial^2 G_5}{\partial r\partial\psi}} - \frac{1}{r^2}\widehat{\frac{\partial G_5}{\partial\psi}}\right](\boldsymbol{y},\omega\,|\,\boldsymbol{x}), \tag{A 10f}$$

$$\hat{I}_{1\psi}(\boldsymbol{y},\omega\,|\,\boldsymbol{x}) = -\mathrm{i}\frac{\cos\theta}{k_\infty}\frac{1}{(1-M(r)\cos\theta)^2}\frac{1}{r}\widehat{\frac{\partial G_5}{\partial\psi}}(\boldsymbol{y},\omega\,|\,\boldsymbol{x}), \tag{A 10g}$$

$$\hat{I}_{r\psi}(\boldsymbol{y},\omega\,|\,\boldsymbol{x}) = \frac{1}{k_\infty^2(1-M(r)\cos\theta)^2}\left[\frac{1}{r}\widehat{\frac{\partial^2 G_5}{\partial r\partial\psi}} - \frac{1}{r^2}\widehat{\frac{\partial G_5}{\partial\psi}} + \frac{2\,\mathrm{d}M(r)/\mathrm{d}r\ \cos\theta}{(1-M(r)\cos\theta)}\frac{1}{r}\widehat{\frac{\partial G_5}{\partial\psi}}\right], \tag{A 10h}$$

$$\hat{I}_{\psi\psi}(\boldsymbol{y},\omega\,|\,\boldsymbol{x}) = \frac{(\gamma-1)}{2}\hat{G}_5(\boldsymbol{y},\omega\,|\,\boldsymbol{x}) + \frac{1}{k_\infty^2(1-M(r)\cos\theta)^2}\left[\frac{1}{r}\widehat{\frac{\partial G_5}{\partial r}} + \frac{1}{r^2}\widehat{\frac{\partial^2 G_5}{\partial \psi^2}}\right](\boldsymbol{y},\omega\,|\,\boldsymbol{x}). \quad (A\,10i)$$

### A.3. *Numerical evaluation*

The numerical evaluation of (A 10) is fairly straightforward. The radial derivatives are computed by central differencing and, therefore, remain second-order accurate. For example, consider a function $f$ defined at the radial location $r(i)$, which may itself represent the Green's function, $\hat{G}_5[r_{(i)}]$, or the Mach-number profile, $M[r_{(i)}]$. Using the central difference formula, the derivative is defined by $\mathrm{d}f(i)/\mathrm{d}r = [f(i+1) - f(i-1)]/2r(i)$. However, in order to define the derivative at the boundary points of the grid (at $i=1$ and $i=N$), we construct a small parabola about the nearest set of points; for example, the derivative at $i=1$ is found by constructing a parabola about the points at $i=(1,2,3)$; and in a similar way the derivative at $i=N$ is found by constructing a parabola about $i=(N-2, N-1, N)$.

It is important to note, however, that we only need to differentiate terms like $\mathrm{d}M(r)/\mathrm{d}r$ and $\partial\hat{G}_5/\partial r$. There is a second-order derivative of $\hat{G}_5$ (i.e. $\partial^2\hat{G}_5/\partial r^2$) in the term $\hat{I}_{rr}(\boldsymbol{y},\omega\,|\,\boldsymbol{x})$, but, as it happens, we can rewrite the whole $\hat{I}_{rr}$ term exactly by deriving an equation for the Laplacian of $\hat{G}_5$. If we eliminate the Green's function variable $G_j$ in A3–A4, we obtain an explicit wave equation that we can re-arrange to isolate the Laplacian $\partial^2\hat{G}_5/\partial y_j^2$. The formula that follows can be written as

$$\widetilde{\nabla}^2\widetilde{G}_5(r,k,m,\omega\,|\,\boldsymbol{x}) = -\left[k_\infty^2\left(1+M(r)\frac{k}{k_\infty}\right)^2\widetilde{G}_5 + 2\left(1+M(r)\frac{k}{k_\infty}\right)\times\frac{\partial}{\partial r}\left\{\frac{1}{\left(1+M(r)\dfrac{k}{k_\infty}\right)}\right\}\frac{\partial\widetilde{G}_5}{\partial r}\right], \quad (A\,11)$$

where the Fourier transform of the Laplacian operator ($\widetilde{\nabla}^2$) is defined by

$$\widetilde{\nabla}^2 = \frac{1}{r}\frac{\partial}{\partial r}\left\{r\frac{\partial}{\partial r}\right\} - k_\infty^2 k^2 - \frac{m^2}{r^2}.$$

Before we can actually use this to simplify $\hat{I}_{rr}(\boldsymbol{y},\omega\,|\,\boldsymbol{x})$, however, we have to take the inverse Fourier transform in $k$ (using the method of stationary phase) and the inverse Fourier transform in angular order $m$ (expanding as a Fourier series). When we apply the inverse transforms, we can use the 'wide hat' notation again to write an equation for the wide-hat-of-$\nabla^2 G_5$, evaluated at the axial wavenumber $k=-k_\infty\cos\theta$. Now we return to $\hat{I}_{rr}(\boldsymbol{y},\omega\,|\,\boldsymbol{x})$. In (A 10) we defined it as

$$\hat{I}_{rr}(\boldsymbol{y},\omega\,|\,\boldsymbol{x}) = \frac{(\gamma-1)}{2}\hat{G}_5(\boldsymbol{y},\omega\,|\,\boldsymbol{x}) + \underbrace{\frac{1}{k_\infty^2(1-M(r)\cos\theta)^2}\left[\widehat{\frac{\partial^2 G_5}{\partial r^2}} + \frac{2\mathrm{d}M(r)/\mathrm{d}r\,\cos\theta}{(1-M(r)\cos\theta)}\widehat{\frac{\partial G_5}{\partial r}}\right]}_{\text{rewrite using the Laplacian of } \hat{G}_5}(\boldsymbol{y},\omega\,|\,\boldsymbol{x}). \quad (A\,12)$$

We can now rewrite the term that appears under the brace using the expression for the Laplacian of $G_5$ in (A 11) to show that

$$\hat{I}_{rr}(\boldsymbol{y},\omega\,|\,\boldsymbol{x}) = \frac{(\gamma-1)}{2}\hat{G}_5(\boldsymbol{y},\omega\,|\,\boldsymbol{x}) - \frac{1}{k_\infty^2(1-M(r)\cos\theta)^2} \times \left[k_\infty^2(1-M(r)\cos\theta)^2\hat{G}_5 + \frac{1}{r}\widehat{\frac{\partial G_5}{\partial r}} - k_\infty^2\cos^2\theta\;\hat{G}_5 + \frac{1}{r^2}\widehat{\frac{\partial^2 G_5}{\partial\psi^2}}\right]. \quad \text{(A 13)}$$

Hence, the radial differentiation only involves $\partial G_5/\partial r$-like terms.

### A.4. *Expression for the trace of the wave propagation tensor*

The trace of the second-rank wave propagation tensor $\hat{I}_{jj}(\boldsymbol{y},\omega\,|\,\boldsymbol{x})$ can be simplified to reveal a rather interesting result. Since $\hat{I}_{jj} = \hat{I}_{11} + \hat{I}_{rr} + \hat{I}_{\psi\psi}$, we can use (A 10), and the already simplified version of $\hat{I}_{rr}$ given by (A 13), to define the trace term exactly:

$$\begin{aligned}\hat{I}_{jj}(\boldsymbol{y},\omega\,|\,\boldsymbol{x}) &= \left[\hat{I}_{11} + \hat{I}_{rr} + \hat{I}_{\psi\psi}\right](\boldsymbol{y},\omega\,|\,\boldsymbol{x}) \\ &= \left[\frac{(\gamma-1)}{2}\hat{G}_5 + \frac{(\gamma-1)M(r)\cos\theta}{(1-M(r)\cos\theta)}\hat{G}_5 - \frac{\cos^2\theta}{(1-M(r)\cos\theta)^2}\hat{G}_5\right] \\ &\quad + \frac{(\gamma-1)}{2}\hat{G}_5 \; + - \frac{1}{k_\infty^2(1-M(r)\cos\theta)^2} \\ &\quad \times \left[k_\infty^2(1-M(r)\cos\theta)^2\hat{G}_5 + \frac{1}{r}\widehat{\frac{\partial G_5}{\partial r}} - k_\infty^2\cos^2\theta\;\hat{G}_5 + \frac{1}{r^2}\widehat{\frac{\partial^2 G_5}{\partial\psi^2}}\right] \\ &\quad + \frac{(\gamma-1)}{2}\hat{G}_5 + \frac{1}{k_\infty^2(1-M(r)\cos\theta)^2}\left[\frac{1}{r}\widehat{\frac{\partial G_5}{\partial r}} + \frac{1}{r^2}\widehat{\frac{\partial^2 G_5}{\partial\psi^2}}\right]. \end{aligned} \quad \text{(A 14)}$$

After simplifying, we can easily show $\hat{I}_{jj}(\boldsymbol{y},\omega\,|\,\boldsymbol{x}) \propto \hat{G}_5(\boldsymbol{y},\omega\,|\,\boldsymbol{x})$, since

$$\hat{I}_{jj}(\boldsymbol{y},\omega\,|\,\boldsymbol{x}) = \left[\left(\frac{3}{2} + \frac{M(r)\cos\theta}{(1-M(r)\cos\theta)}\right)(\gamma-1) - 1\right]\hat{G}_5(\boldsymbol{y},\omega\,|\,\boldsymbol{x}). \quad \text{(A 15)}$$

The adjoint energy equation, given by (A 3), shows that $\hat{G}_5$ is proportional to $\widehat{\partial G_j/\partial y_j}$. Now, since the trace of the symmetric second-rank propagation is identical to $\hat{I}_{jj}$ (i.e. $\hat{I}^{sym}_{jj} = \hat{I}_{jj}$), (A 15) implies: $\hat{I}^{sym}_{jj}(\boldsymbol{y},\omega\,|\,\boldsymbol{x}) \propto \widehat{\partial G_j/\partial y_j}(\boldsymbol{y},\omega\,|\,\boldsymbol{x})$. This is an important result because we show in Appendix B that at very low frequencies, the convective derivative of the pressure-like Green's function ($\hat{G}_5$ in our solution) will remain $O(\omega^2)$. Hence, the trace of the second-rank wave propagation tensor will also remain $O(\omega^2)$ at very low frequencies – or $\hat{I}^{sym}_{jj} = O(\omega^2)$ in the limit as $\omega \to 0$.

### A.5. *Numerical analysis*

In this section, we conduct two robustness checks. First, we assess the accuracy of the differentiability of $\hat{G}_5$ by computing the OASPL when the wave propagation term is $\hat{I}^{sym}_{jjkk}(\boldsymbol{y},\omega\,|\,\boldsymbol{x}) = \hat{I}^{sym}_{jj}(\boldsymbol{y},\omega\,|\,\boldsymbol{x})\hat{I}^{sym}_{kk}(\boldsymbol{y},-\omega\,|\,\boldsymbol{x})$ (as in the case of instantaneous isotropy, (3.3)). We can then compare the direct numerical evaluation of $\hat{I}^{sym}_{jjkk}$ using (A 10) (which defines each component of $\hat{I}_{ij}$) and (2.20), to the exact 'analytical' formula for $\hat{I}^{sym}_{jjkk}$ using $\hat{I}^{sym}_{jj}(\boldsymbol{y},\omega\,|\,\boldsymbol{x})$ given by (A 15). Remember, the robustness of solving the Green's function problem for a parallel shear layer in terms of $\hat{G}_5(\boldsymbol{y},\omega\,|\,\boldsymbol{x})$ has already been proved by Afsar (2009). In figure 5(*a*), we show that OASPL predictions by the

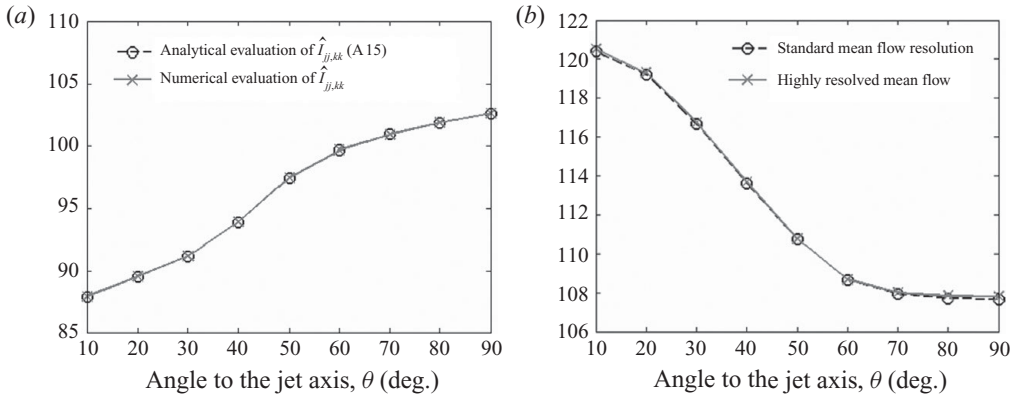


FIGURE 5. Numerical checks on OASPL (dB) calculations. OASPL (dB) versus observation angle (deg.). (*a*) Differentiability of the Green's function; the coefficients $(c_l, c_\tau, A)$ are the same as in figure 1. (*b*) Convergence of statistical isotropy (4.3), momentum transfer component only; the coefficients $(c_l, c_\tau, A)$ are the same as in figure 2.

analytical formula (A 10) and numerical evaluation of $\hat{I}^{sym}_{jjkk}$ are very nearly identical (where the mean flow resolution is 88 points in the radial direction).

The second test we do here is to assess the convergence of the OASPL calculation for statistical isotropy (4.3). We need only consider the momentum transfer part of (4.3) since it causes the increase in OASPL at small observation angles. We assess the convergence of the calculation using the mesh enrichment algorithm described in Afsar (2009). That is, we compute the quadratic forms in the integrand of (4.3), $\hat{I}^{sym}_{jkjk}$ and $\hat{I}^{sym}_{jjkk}$, at a high resolution of 3000 nodes in the radial direction, and then interpolate back to the original grid (quadratically) to compute the integrand and evaluate the integral. This is then compared to a calculation of the quadratic forms on the standard grid resolution (88 points radially). The calculation is well converged and is shown in figure 5(*b*).

## Appendix B. low-frequency asymptotics

### B.1. *Wave equation*

In this Appendix, we determine the leading-order behaviour of $\hat{G}_5(\boldsymbol{y}, \omega \,|\, \boldsymbol{x})$ when the frequency is very low. It turns out to be much simpler to do this when the field point $\boldsymbol{y}$ is described through Cartesian coordinates. We begin by manipulating (A 3) and (A 4) to get an explicit wave equation for $\hat{G}_5(\boldsymbol{y}, \omega \,|\, \boldsymbol{x})$, viz

$$\frac{\hat{\mathrm{D}}_1^3 \hat{G}_5}{\mathrm{D}\tau^3} - \frac{\partial}{\partial y_j}\left\{\tilde{c}^2 \frac{\hat{\mathrm{D}}_1}{\mathrm{D}\tau}\frac{\partial \hat{G}_5}{\partial y_j}\right\} + 3\tilde{c}^2 \frac{\partial U}{\partial y_j}\frac{\partial^2 \hat{G}_5}{\partial y_j \partial y_1} = \frac{\hat{\mathrm{D}}_1^3}{\mathrm{D}\tau^3}\delta(\boldsymbol{y}-\boldsymbol{x}). \tag{B 1}$$

The convective derivative is defined by $\hat{\mathrm{D}}_1/\mathrm{D}\tau \equiv \mathrm{i}\omega + U(\boldsymbol{y}_\perp)\partial/\partial y_1$; and by definition the mean field is given by $\tilde{c}^2 = \tilde{c}^2(\boldsymbol{y}_\perp)$ and $U = U(\boldsymbol{y}_\perp)$ with $\boldsymbol{y}_\perp$ being the transverse spatial coordinate $\boldsymbol{y}_\perp = (y_2, y_3)$. Now we perform a simple re-arrangement on the second term in (B 1) to isolate the Laplacian expression $\partial^2 \hat{G}_5/\partial y_j^2$. If we use the commutative relation

$$\frac{\partial}{\partial y_j}\frac{\hat{\mathrm{D}}_1 \hat{G}_5}{\mathrm{D}\tau} = \frac{\hat{\mathrm{D}}_1}{\mathrm{D}\tau}\frac{\partial \hat{G}_5}{\partial y_j} + \frac{\partial U}{\partial y_j}\frac{\partial \hat{G}_5}{\partial y_1},$$

we can easily show that

$$\frac{\hat{\mathrm{D}}_1^3\hat{G}_5}{\mathrm{D}\tau^3}-\tilde{c}^2\frac{\hat{\mathrm{D}}_1}{\mathrm{D}\tau}\frac{\partial^2\hat{G}_5}{\partial y_j^2}-\frac{\partial\tilde{c}^2}{\partial y_j}\frac{\hat{\mathrm{D}}_1}{\mathrm{D}\tau}\frac{\partial\hat{G}_5}{\partial y_j}+2\tilde{c}^2\frac{\partial U}{\partial y_j}\frac{\partial^2\hat{G}_5}{\partial y_j\partial y_1}=\frac{\hat{\mathrm{D}}_1^3}{\mathrm{D}\tau^3}\delta(\boldsymbol{y}-\boldsymbol{x}),\qquad(\mathrm{B}\,2)$$

where suffix $j=(1,2,3)$.

Now we take Fourier transforms in $y_1$ (where $\partial/\partial y_1\rightarrow \mathrm{i}k$ after integrating by parts). This gives a wave equation for $\widetilde{G}_5(\boldsymbol{y}_\perp,k,\omega\,|\,\boldsymbol{x})$, which after some algebraic manipulation can be written in the following very simple way:

$$\nabla_\perp^2\widetilde{G}_5(\boldsymbol{y}_\perp,\hat{k},k_\infty\,|\,\boldsymbol{x})+\left[k_\infty^2q^2(\boldsymbol{y}_\perp,\hat{k})+\mathrm{Ł}(\boldsymbol{y}_\perp,\hat{k})\right]\widetilde{G}_5(\boldsymbol{y}_\perp,\hat{k},k_\infty\,|\,\boldsymbol{x})$$
$$=k_\infty^2\chi^2\delta(\boldsymbol{y}_\perp-\boldsymbol{x}_\perp)\,\mathrm{e}^{-\mathrm{i}k_\infty\hat{k}x_1},\qquad(\mathrm{B}\,3)$$

where $k_\infty=\omega/c_\infty$, $\hat{k}=k/k_\infty$, $a_r(\boldsymbol{y}_\perp)=\tilde{c}(\boldsymbol{y}_\perp)/c_\infty$ and $D(\boldsymbol{y}_\perp,\hat{k})=1+M(\boldsymbol{y}_\perp)\hat{k}$. The term $q^2(\boldsymbol{y}_\perp,\hat{k})$ is defined by $q^2(\boldsymbol{y}_\perp,\hat{k})=\chi^2-\hat{k}^2$, where $\chi=D/a_r$. If we define the transverse component of the gradient operator as $\nabla_\perp\equiv\boldsymbol{e}_2\partial/\partial y_2+\boldsymbol{e}_3\partial/\partial y_3$, we can define the transverse part of the Laplacian by the scalar operator, $\nabla_\perp^2$, or $\nabla_\perp^2\equiv\partial^2/\partial y_2^2+\partial^2/\partial y_3^2$. Moreover, the operator $\mathrm{Ł}(\boldsymbol{y}_\perp,\hat{k})$ is given by $\mathrm{Ł}(\boldsymbol{y}_\perp,\hat{k})=2\chi\nabla_\perp[1/\chi]\cdot\nabla_\perp\{\ldots\}$. Equation (B 3) is identical to (2.8) in Goldstein (1982), if we replace $G_5$ by the adjoint Lilley Green's function, $G_a$, where $G_5=-D_1^3G_a/\mathrm{D}\tau^3$ (this correspondence is derived in Afsar 2008, Appendix C). We shall leave $a_r(\boldsymbol{y}_\perp)\neq1$, because it does not add much complication here. Also remember that for all $(\boldsymbol{y}_\perp,\hat{k})$, the mean flow term $D(\boldsymbol{y}_\perp,\hat{k})$ is non-zero in subsonic flows where critical layers do not exist, so that $D^{-1}$ is non-singular.

Equation (B 3) possesses two length scales: the nozzle exit diameter, $D_{jet}$, which characterizes the transverse variation of the mean flow and the acoustic wavelength through $k_\infty^{-1}$ characterizing the wave propagation (since $k_\infty^{-1}=\lambda_{acoustic}/2\pi$). In low-frequency asymptotic problems, the perturbation parameter is defined by the Helmholtz number $\epsilon=(k_\infty D_{jet})$. As $\epsilon\rightarrow0$, the scales defined through the product $(k_\infty D_{jet})$ become asymptotically disparate. That is, when $\epsilon\rightarrow0$, $\lambda_{acoustic}$ becomes very large relative to the transverse variation of the mean flow.

This problem is a singular perturbation problem because at large values of $\boldsymbol{y}_\perp$, where $\widetilde{G}_5$ satisfies the (adjoint) radiation condition, the solution is transcendental and bounded (zero) at infinity. This behaviour must be made to agree with $\widetilde{G}_5$ at smaller values of $\boldsymbol{y}_\perp$, i.e. when $\boldsymbol{y}_\perp$ is held fixed and non-dimensionalized so that it remains $O(1)$. Hence, for a given value of $(\hat{k}\,|\,\boldsymbol{x})$, a single asymptotic expansion for $\widetilde{G}_5$, such as $\widetilde{G}_5(\boldsymbol{y}_\perp,\epsilon)=g_5^{(0)}(\boldsymbol{y}_\perp)+\epsilon g_5^{(1)}(\boldsymbol{y}_\perp)+\epsilon^2g_5^{(2)}(\boldsymbol{y}_\perp)+o(\epsilon^2)$, would not hold for all values of $\boldsymbol{y}_\perp$. But this type of non-uniformity in $\widetilde{G}_5$ would still exist when $\omega=O(1)$. In that case, as Afsar (2009) showed, a numerical solution for $\widetilde{G}_5$ can easily be found using the patching method. The low-frequency limit, however, allows a uniformly valid analytical solution to be constructed using the method of matched asymptotic expansions, and for which we are only interested in the leading-order behaviour. We proceed by first defining an inner region and an outer region.

### B.2. *Inner and outer regions*

We follow the example problem in Crighton *et al.* (1992), and begin by normalizing the spatial coordinate $\boldsymbol{y}_\perp=(y_2,y_3)$ to assess the size of each term in (B 3) consistently. It seems natural to use $k_\infty^2$. If we now introduce a dimensionless spatial coordinate, $\hat{\boldsymbol{y}}_\perp$, defined by $\hat{\boldsymbol{y}}_\perp=k_\infty\boldsymbol{y}_\perp$, and where the gradient operator becomes, $\hat{\nabla}_\perp=(1/k_\infty)\nabla_\perp$.

Then, (B 3) transforms to

$$\hat{\nabla}_\perp^2 \widetilde{G}_5(\hat{\boldsymbol{y}}_\perp/k_\infty, \hat{k}, k_\infty \,|\, \hat{\boldsymbol{x}}/k_\infty) + \left[q^2(\hat{\boldsymbol{y}}_\perp/k_\infty, \hat{k}) + \widehat{\mathrm{L}}(\hat{\boldsymbol{y}}_\perp/k_\infty, \hat{k})\right] \times \widetilde{G}_5(\hat{\boldsymbol{y}}_\perp/k_\infty, \hat{k}, k_\infty \,|\, \hat{\boldsymbol{x}}/k_\infty) = \frac{\chi^2}{k_\infty}\delta(\hat{\boldsymbol{y}}_\perp - \hat{\boldsymbol{x}}_\perp)\, \mathrm{e}^{-\mathrm{i}\hat{k}\hat{x}_1}. \quad \text{(B 4)}$$

This is now in a form ready for asymptotic expansion. Since the dimensionless outer spatial coordinate is $\hat{\boldsymbol{y}}_\perp = (\hat{y}_2, \hat{y}_3)$, the Green's function $\widetilde{G}_5$ in the outer region is given by (B 5*a*)

$$\widetilde{G}_5(\boldsymbol{y}_\perp, \hat{k}, k_\infty \,|\, \boldsymbol{x}) = \widetilde{G}_5(\hat{\boldsymbol{y}}_\perp/k_\infty, \hat{k}, k_\infty \,|\, \hat{\boldsymbol{x}}/k_\infty) = \widetilde{G}_5^o(\hat{\boldsymbol{y}}_\perp, \epsilon, \hat{k} \,|\, \hat{\boldsymbol{x}}), \quad \text{(B 5a)}$$

$$\widetilde{G}_5(\boldsymbol{y}_\perp, \hat{k}, k_\infty \,|\, \boldsymbol{x}) = \widetilde{G}_5(\hat{\boldsymbol{Y}}_\perp D_{jet}, \hat{k}, k_\infty \,|\, \hat{\boldsymbol{x}}/k_\infty) = \widetilde{G}_5^i(\hat{\boldsymbol{Y}}_\perp, \epsilon, \hat{k} \,|\, \hat{\boldsymbol{x}}), \quad \text{(B 5b)}$$

where the superscript '*o*' on $\widetilde{G}_5$ refers to the outer region. Similarly, in the inner region, the spatial coordinate is $\hat{\boldsymbol{Y}}_\perp = (\hat{Y}_2, \hat{Y}_3)$, and is defined by $\hat{\boldsymbol{Y}}_\perp = \hat{\boldsymbol{y}}_\perp/\epsilon$. If we denote the inner region with the superscript '*i*', the Green's function $\widetilde{G}_5$ can be expressed as (B 5*b*). Now, for a given $(\hat{k} \,|\, \hat{\boldsymbol{x}})$, the inner expansion $\widetilde{G}_5^i(\hat{\boldsymbol{Y}}_\perp, \epsilon, \hat{k} \,|\, \hat{\boldsymbol{x}})$ is valid in a region where $\hat{\boldsymbol{y}}_\perp = O(\epsilon)$, i.e. at $\hat{\boldsymbol{Y}}_\perp = O(1)$. On the other hand, the outer $\widetilde{G}_5^o(\hat{\boldsymbol{y}}_\perp, \epsilon, \hat{k} \,|\, \hat{\boldsymbol{x}})$ is valid for large values of $\hat{\boldsymbol{y}}_\perp$ extending from $\epsilon$, where $\hat{\boldsymbol{y}}_\perp = O(\epsilon)$, right out to infinity. Hence, at some intermediate region in $\hat{\boldsymbol{y}}_\perp$ both expansions must overlap. We can avoid trial and error in the choice of gauge function for the asymptotic expansion in the inner region if we actually start with the outer region to begin with. The inner expansion will break down at large distances from the jet where $\hat{\boldsymbol{Y}}_\perp \neq O(1)$, and where the Green's function $\widetilde{G}_5$ possesses transcendental behaviour to satisfy the boundary condition at infinity. Hence, if any logarithmic terms appear in the outer expansion, we must include them in the inner expansion at the appropriate order of $\epsilon$.

### B.3. *The outer expansion,* $\widetilde{G}_5^o(\hat{\boldsymbol{y}}_\perp, \epsilon, \hat{k} \,|\, \hat{\boldsymbol{x}})$

This corresponds to the Green's function which is valid at large distances from the jet; i.e. as the outer variable, $|\, \hat{\boldsymbol{y}}_\perp \,| \to \infty$, and in which case the mean flow is constant and any gradients of the mean flow are zero. The field (B 4) reduces to the ordinary Helmholtz equation. Since the outer region represents the solution to the Green's function right out to infinity, we can simplify the mean flow terms in (B 4), because they are no longer a function of $\hat{\boldsymbol{y}}_\perp$; i.e. $D(\hat{k}) = 1$ and $a_r(\boldsymbol{y}_\perp) = 1$, so that $q^2(\hat{k}) = 1 - \hat{k}^2$, since $M_\infty = 0$. Hence, the field equation we must solve in the outer region is simply

$$\nabla_\perp^2 \widetilde{G}_5^o(\hat{\boldsymbol{y}}_\perp, \epsilon, \hat{k} \,|\, \hat{\boldsymbol{x}}) + q^2(\hat{k})\widetilde{G}_5^o(\hat{\boldsymbol{y}}_\perp, \epsilon, \hat{k} \,|\, \hat{\boldsymbol{x}}) = \frac{1}{k_\infty}\delta(\hat{\boldsymbol{y}}_\perp - \hat{\boldsymbol{x}}_\perp)\, \mathrm{e}^{-\mathrm{i}\hat{k}\hat{x}_1}. \quad \text{(B 6)}$$

At this point, we would start the usual technique in perturbation analysis of replacing $\widetilde{G}_5^o$ by a Poincaré series in integral powers of the parameter $\epsilon$ in the particular manner that $\widetilde{G}_5^o = G_5^{(0)} + \epsilon G_5^{(1)} + \epsilon^2 G_5^{(2)} + o(\epsilon^2)$, and then to solve for each order by holding $\hat{\boldsymbol{y}}_\perp$ fixed. However, this is not necessary here because (B 6) is independent of $\epsilon$ since the differential operator on the left-hand side does not have any $\epsilon$ terms, in which case we are actually solving the dimensional field equation, given by (B 3), when $|\, \boldsymbol{y}_\perp \,| \to \infty$. We can then re-arrange (B 3) slightly to show

$$\left[\nabla_\perp^2 + k_\infty^2 q^2(\hat{k})\right]\left\{-4\pi\frac{\mathrm{e}^{\mathrm{i}k_\infty \hat{k} x_1}}{k_\infty^2}\widetilde{G}_5\right\} = -4\pi\delta(\boldsymbol{y}_\perp - \boldsymbol{x}_\perp). \quad \text{(B 7)}$$

This differential operator is now self-adjoint, reciprocity holds and $\widetilde{G}_5(\boldsymbol{y}\,|\,\boldsymbol{x}) = \widetilde{G}_5(\boldsymbol{x}\,|\,\boldsymbol{y})$. The solution to (B 7) is given in Morse & Feshbach (1953, p. 891). That is

$$\left\{-4\pi\frac{\mathrm{e}^{\mathrm{i}k_\infty\hat{k}x_1}}{k_\infty^2}\widetilde{G}_5\right\} = \mathrm{i}\pi H_0^{(1)}(k_\infty q\,|\,\boldsymbol{y}_\perp - \boldsymbol{x}_\perp\,|). \tag{B 8}$$

In terms of the outer variable $\hat{\boldsymbol{y}}_\perp$, however, the solution for $\widetilde{G}_5^o(\hat{\boldsymbol{y}}_\perp, \epsilon, \hat{k}\,|\,\boldsymbol{x})$ is

$$\widetilde{G}_5^o(\hat{\boldsymbol{y}}_\perp, \epsilon, \hat{k}\,|\,\boldsymbol{x}) = -\frac{\mathrm{i}k_\infty^2}{4}\mathrm{e}^{-\mathrm{i}k_\infty\hat{k}x_1}H_0^{(1)}(q\,|\,\hat{\boldsymbol{y}}_\perp - k_\infty\boldsymbol{x}_\perp\,|), \tag{B 9}$$

where $q^2(\hat{k}) = 1 - \hat{k}^2$. Equation (B 9) represents the particular solution to (B 7) – but in order to match the scattered wave to the inner, we must include the solution to the homogeneous equation (when the right-hand side of (B 7) is zero) as well. Since the homogeneous solution must be of the same algebraic order in $k_\infty$ as the particular solution in (B 9), we write it as $k_\infty^2\beta(\hat{k}\,|\,\boldsymbol{x})H_0^{(1)}(q\,|\,\hat{\boldsymbol{y}}_\perp|)$. The Green's function $\widetilde{G}_5^o(\hat{\boldsymbol{y}}_\perp, \epsilon, \hat{k}\,|\,\boldsymbol{x})$ is then

$$\widetilde{G}_5^o(\hat{\boldsymbol{y}}_\perp, \epsilon, \hat{k}\,|\,\boldsymbol{x}) = k_\infty^2\beta(\hat{k}\,|\,\boldsymbol{x})H_0^{(1)}(q\,|\,\hat{\boldsymbol{y}}_\perp|) - \frac{\mathrm{i}k_\infty^2}{4}\mathrm{e}^{-\mathrm{i}k_\infty\hat{k}x_1}H_0^{(1)}(q\,|\,\hat{\boldsymbol{y}}_\perp - k_\infty\boldsymbol{x}_\perp\,|). \tag{B 10}$$

Solution (B 10) is consistent with the Green's function solution given by Dowling *et al.* (1978, equation (4.5)) for the pressure-like Green's function in cylindrical coordinates since the addition theorem for cylinder functions (Morse & Feshbach 1953, equation (7.2.51)) can be used to show that

$$H_0^{(1)}(k_\infty q\,|\,\boldsymbol{y}_\perp - \boldsymbol{x}_\perp\,|) = \sum_{m=-\infty}^{m=+\infty} J_m(k_\infty q r)H_m^{(1)}(k_\infty q R)\,\mathrm{e}^{\mathrm{i}m(\psi-\Psi)}, \tag{B 11}$$

where, in cylindrical coordinates, $\boldsymbol{y}_\perp = (r, \psi)$ and $\boldsymbol{x}_\perp = (R, \Psi)$. This, therefore, has the same basic structure as the solution in (4.5) in Dowling *et al.* (1978). The term, $H_0^{(1)}(q\,|\,\hat{\boldsymbol{y}}_\perp|)$ in (B 10) has incoming wave behaviour at infinity in the outer variable. Dowling *et al.* (1978) showed that this implies that, when real, $q(\hat{k})$ must carry the sign of $\omega$, but when it is complex, its imaginary part must be positive so that $\widetilde{G}_5^o(\hat{\boldsymbol{y}}_\perp, \epsilon, \hat{k}\,|\,\boldsymbol{x})$ remains $O(1)$ as $|\,\hat{\boldsymbol{y}}_\perp\,| \to \infty$. Both of these conditions are satisfied by a Riemann sheet in the complex $k$-plane, where $\mathrm{Im}\,(q) = 0$, such that there is a branch cut along the real axis, from 1 to $+\infty$, and from $-1$ to $-\infty$.

Now $|\,\boldsymbol{y}_\perp - \boldsymbol{x}_\perp\,| = x_\perp - \boldsymbol{x}_\perp\cdot\boldsymbol{y}_\perp/x_\perp + O(x_\perp^{-1})$ as $x_\perp \to \infty$, where $x_\perp = |\,\boldsymbol{x}_\perp\,|$, since the field point $\boldsymbol{x}_\perp$ is at infinity. Hence, we can write (B 10) as

$$\widetilde{G}_5^o(\hat{\boldsymbol{y}}_\perp, \epsilon, \hat{k}\,|\,\boldsymbol{x}) = k_\infty^2\beta(\hat{k}\,|\,\boldsymbol{x})H_0^{(1)}(q\,|\,\hat{\boldsymbol{y}}_\perp|) - \frac{\mathrm{i}k_\infty^2}{4}\,\mathrm{e}^{-\mathrm{i}k_\infty\hat{k}x_1}H_0^{(1)}\left[qk_\infty x_\perp - q\frac{\boldsymbol{x}_\perp\cdot\hat{\boldsymbol{y}}_\perp}{x_\perp}\right]. \tag{B 12}$$

Under the matching procedure, we first rewrite the outer variable in terms of the inner variable, $\hat{\boldsymbol{y}}_\perp = \epsilon\hat{\boldsymbol{Y}}_\perp$. The first term in (B 12) has a logarithmic singularity as $\epsilon \to 0$. On the other hand, the argument of the Hankel function in the second term in (B 12) becomes $(qk_\infty x_\perp - \epsilon q A)$, where $A = \boldsymbol{x}_\perp\cdot\hat{\boldsymbol{Y}}_\perp/x_\perp$ and $A = O(1)$. The term $(qk_\infty x_\perp - \epsilon q A)$ is of large magnitude even though the frequency is low. This is because $k_\infty x_\perp \propto x_\perp/\lambda_{acoustic}$, and $x_\perp \to \infty$, whereas $\lambda_{acoustic}$ is large, but only relative to the transverse variation of the mean flow, defined by the transverse length scale $D_{jet}$. So, for this reason, we express the solution in (B 12) in terms of $\hat{\boldsymbol{x}} = k_\infty\boldsymbol{x}$, where $|\,\hat{\boldsymbol{x}}\,| \to \infty$. Now we can replace the Hankel function in the second term by its

large argument form (Lebedev 1972, p. 135), and leave the $\epsilon qA$ term as a small correction. Hence,

$$\widetilde{G}_5^o(\epsilon\hat{\boldsymbol{Y}}_\perp,\epsilon,\hat{k}\,|\,\hat{\boldsymbol{x}}) = \mp\mathrm{i}\frac{2\epsilon^2}{\pi D_{jet}^2}\beta(\hat{k}\,|\,\hat{\boldsymbol{x}})\ln\frac{2}{q\epsilon\,|\,\hat{\boldsymbol{Y}}_\perp\,|} - \frac{\mathrm{i}\epsilon^2}{4D_{jet}^2}\,\mathrm{e}^{\mathrm{i}q\hat{x}_\perp-\mathrm{i}\hat{k}\hat{x}_1-\mathrm{i}\pi/4}\left[\frac{2}{\pi q}\right]^{1/2} f(\hat{\boldsymbol{Y}}_\perp,\epsilon,\hat{k}\,|\,\hat{\boldsymbol{x}}), \quad \text{(B 13)}$$

where $f(\hat{\boldsymbol{Y}}_\perp,\epsilon,\hat{k}\,|\,\hat{\boldsymbol{x}}) = (\hat{x}_\perp-\epsilon A)^{-(1/2)}\,\mathrm{e}^{-\mathrm{i}\epsilon qA}$. We can now take the limit as $\epsilon\to 0$ and expand this term by first expanding $(\hat{x}_\perp-\epsilon A)^{-(1/2)}$ and $\mathrm{e}^{-\mathrm{i}\epsilon qA}$ individually, and then multiplying the expansions together. Hence

$$f(\hat{\boldsymbol{Y}}_\perp,\epsilon,\hat{k}\,|\,\hat{\boldsymbol{x}}) = \frac{1}{\sqrt{\hat{x}_\perp}} - \mathrm{i}qA\left(\frac{\epsilon}{\sqrt{\hat{x}_\perp}}\right) + O\left(\epsilon/\hat{x}_\perp^{3/2}\right). \quad \text{(B 14)}$$

Now if we substitute this back into (B 13), and use the notation from Nayfeh (1972, chap. 4) to signify that this is now the inner limit of the outer expansion $[\widetilde{G}_5^o]^{(i)}$, we have

$$[\widetilde{G}_5^o]^{(i)}(\epsilon\hat{\boldsymbol{Y}}_\perp,\epsilon,\hat{k}\,|\,\hat{\boldsymbol{x}}) = \epsilon^2\overline{\beta}(\hat{k}\,|\,\hat{\boldsymbol{x}})\left[\ln\frac{2}{q\,|\,\hat{\boldsymbol{Y}}_\perp\,|} - \ln\epsilon\right] + \epsilon^2 C(\hat{k}\,|\,\hat{\boldsymbol{x}})\,[1-\mathrm{i}\epsilon qA], \quad \text{(B 15)}$$

where $\overline{\beta}(\hat{k}\,|\,\hat{\boldsymbol{x}}) = 2\mathrm{i}\beta(\hat{k}\,|\,\hat{\boldsymbol{x}})/\pi D_{jet}^2$, and the term $C(\hat{k}\,|\,\hat{\boldsymbol{x}})$ is also independent of $\hat{\boldsymbol{Y}}_\perp$ and is given by

$$C(\hat{k}\,|\,\hat{\boldsymbol{x}}) = -\frac{\mathrm{i}}{4D_{jet}^2}\,\mathrm{e}^{\mathrm{i}q\hat{x}_\perp-\mathrm{i}\hat{k}\hat{x}_1-\mathrm{i}\pi/4}\left[\frac{2}{\pi q\hat{x}_\perp}\right]^{1/2}. \quad \text{(B 16)}$$

### B.4. *The inner expansion,* $\widetilde{G}_5^i(\hat{\boldsymbol{Y}}_\perp,\epsilon,\hat{k}\,|\,\hat{\boldsymbol{x}})$

The inner expansion corresponds to a series expansion under the limit process of $\epsilon\to 0$ with $\hat{\boldsymbol{Y}}_\perp$ held fixed at $\hat{\boldsymbol{Y}}_\perp = O(1)$. This allows one to magnify a region of the jet around the neighbourhood of $\hat{\boldsymbol{y}}_\perp = O(\epsilon)$. When the outer expansion is projected down to the overlap region (inner limit of the outer expansion), it is identical to when the inner expansion is projected up to the overlap region (outer limit of the inner expansion).

Under the stretched coordinate $\hat{\boldsymbol{Y}}_\perp = \hat{\boldsymbol{y}}_\perp/\epsilon$, the gradient operator is defined by $\epsilon\hat{\nabla}_y = \hat{\nabla}_Y$, where $\hat{\nabla}_Y \equiv \boldsymbol{e}_2\partial/\partial\hat{Y}_2 + \boldsymbol{e}_3\partial/\partial\hat{Y}_3$ (inner) and $\hat{\nabla}_y \equiv \boldsymbol{e}_2\partial/\partial\hat{y}_2 + \boldsymbol{e}_3\partial/\partial\hat{y}_3$ (outer). The mean flow terms in (B 4), $q^2$ and the operator Ł, both depend on $(\hat{\boldsymbol{y}}_\perp/k_\infty,\hat{k})$. In terms of the inner variable, however, this dependence becomes $q^2(\hat{\boldsymbol{Y}}_\perp D_{jet},\hat{k})$ and $Ł(\hat{\boldsymbol{Y}}_\perp D_{jet},\hat{k})$. Hence, the field equation for the Green's function in the inner region is

$$\hat{\nabla}_Y^2\widetilde{G}_5^i(\hat{\boldsymbol{Y}}_\perp,\epsilon,\hat{k}\,|\,\hat{\boldsymbol{x}}) + \left[\epsilon^2 q^2(\hat{\boldsymbol{Y}}_\perp D_{jet},\hat{k}) + \widehat{Ł}(\hat{\boldsymbol{Y}}_\perp D_{jet},\hat{k})\right]\widetilde{G}_5^i(\hat{\boldsymbol{Y}}_\perp,\epsilon,\hat{k}\,|\,\hat{\boldsymbol{x}}) = 0. \quad \text{(B 17)}$$

Here, $\hat{\nabla}_Y^2$ is the transverse component of the Laplacian, where $\hat{\nabla}_Y^2 \equiv \partial^2/\partial\hat{Y}_2^2 + \partial^2/\partial\hat{Y}_3^2$, and in terms of the inner variable, the operator $\widehat{Ł}(\hat{\boldsymbol{Y}}_\perp D_{jet},\hat{k})$ is

$$\widehat{Ł}(\hat{\boldsymbol{Y}}_\perp D_{jet},\hat{k}) = 2\chi\hat{\nabla}_Y\left(\frac{1}{\chi}\right)\cdot\hat{\nabla}_Y\{\ldots\}, \quad \text{(B 18)}$$

where $\chi = \chi(\hat{\boldsymbol{Y}}_\perp D_{jet}, \hat{k})$. Since $\chi^{-1}(\hat{\boldsymbol{Y}}_\perp D_{jet}, \hat{k})$ is non-singular, we can re-arrange the inner field (B 17) in the following form:

$$\hat{\nabla}_Y \cdot \left[\frac{1}{\chi^2}\hat{\nabla}_Y \widetilde{G}_5^i(\hat{\boldsymbol{Y}}_\perp, \epsilon, \hat{k} \,|\, \hat{\boldsymbol{x}})\right] = -\epsilon^2 \left[\frac{q}{\chi}\right]^2 \widetilde{G}_5^i(\hat{\boldsymbol{Y}}_\perp, \epsilon, \hat{k} \,|\, \hat{\boldsymbol{x}}). \tag{B 19}$$

From the inner limit of the outer expansion (B 15), we know the inner expansion must start out as $\epsilon^2(\ln\epsilon)g_5^{(2)} + \cdots$. Hence, we can legitimately pose a Poincaré expansion for $\widetilde{G}_5^i(\hat{\boldsymbol{Y}}_\perp, \epsilon, \hat{k} \,|\, \hat{\boldsymbol{x}})$ to match onto the outer expansion as follows:

$$\widetilde{G}_5^i(\hat{\boldsymbol{Y}}_\perp, \epsilon, \hat{k} \,|\, \hat{\boldsymbol{x}}) = \epsilon^2(\ln\epsilon)g_5^{(1)}(\hat{\boldsymbol{Y}}_\perp, \epsilon, \hat{k} \,|\, \hat{\boldsymbol{x}}) + \epsilon^2 g_5^{(2)}(\hat{\boldsymbol{Y}}_\perp, \epsilon, \hat{k} \,|\, \hat{\boldsymbol{x}}) + \epsilon^3 g_5^{(3)}(\hat{\boldsymbol{Y}}_\perp, \epsilon, \hat{k} \,|\, \hat{\boldsymbol{x}}) + o(\epsilon^3). \tag{B 20}$$

Because the right-hand side of (B 19) has the pre-factor $\epsilon^2$, the term in square brackets on the left-hand side will be $\epsilon^2$ greater than $\widetilde{G}_5^i(\hat{\boldsymbol{Y}}_\perp, \epsilon, \hat{k} \,|\, \hat{\boldsymbol{x}})$. In other words, $\hat{\nabla}_Y \widetilde{G}_5^i(\hat{\boldsymbol{Y}}_\perp, \epsilon, \hat{k} \,|\, \hat{\boldsymbol{x}})$ will always be asymptotically smaller than $\widetilde{G}_5^i(\hat{\boldsymbol{Y}}_\perp, \epsilon, \hat{k} \,|\, \hat{\boldsymbol{x}})$ at very low frequencies. Now if the inner expansion starts out as (B 20), the right-hand side of the inner equation for each order ($\epsilon^2 \ln\epsilon, \epsilon^2, \epsilon^3$) will be zero. So, for a given $(\hat{k} \,|\, \hat{\boldsymbol{x}})$, if we hold the inner variable ($\hat{\boldsymbol{Y}}_\perp$) fixed, each order must satisfy a differential equation of the form

$$\hat{\nabla}_Y \cdot \left[\frac{1}{\chi^2}\hat{\nabla}_Y g_5^{(n)}(\hat{\boldsymbol{Y}}_\perp, \epsilon, \hat{k} \,|\, \hat{\boldsymbol{x}})\right] = 0, \tag{B 21}$$

where $n = (1, 2, 3)$.

### B.5. *Leading-order behaviour*

The leading-order behaviour is simple since we require $g_5^{(2)}(\hat{\boldsymbol{Y}}_\perp, \epsilon, \hat{k} \,|\, \hat{\boldsymbol{x}})$ only, which in order to satisfy (B 21) must be a constant in $\hat{\boldsymbol{Y}}_\perp$ (a similar result was found by Goldstein 1975, equation (16)). Taking the outer limit of the inner expansion and matching this to (B 15) naturally shows $\overline{\beta}(\hat{k} \,|\, \hat{\boldsymbol{x}}) = 0$ and $g_5^{(2)}(\hat{\boldsymbol{Y}}_\perp, \epsilon, \hat{k} \,|\, \hat{\boldsymbol{x}}) = C(\hat{k} \,|\, \hat{\boldsymbol{x}})$. Hence, the uniformly valid solution in the original dimensional field variable $\boldsymbol{y}_\perp = (y_2, y_3)$ is $\hat{G}_5(\boldsymbol{y}_\perp, \omega \,|\, \boldsymbol{x}) = \omega^2 \mathscr{C}(\omega, \boldsymbol{x}) + o(\epsilon)$, where

$$\mathscr{C}(\omega, \boldsymbol{x}) = \frac{D_{jet}^2}{c_\infty^2} \int_{k=-\infty}^{+\infty} C(k/k_\infty, \omega \,|\, \boldsymbol{x})\, \mathrm{e}^{\mathrm{i}ky_1}\, \mathrm{d}k. \tag{B 22}$$

Since $|\boldsymbol{x}| \to \infty$, we can evaluate the $k$-integral in (B 22) quite easily using the method of stationary phase.

## REFERENCES


Afsar, M. Z. 2008 Theory and modelling of jet noise. PhD thesis, Cambridge University, Engineering Department Accession No 50087.

Afsar, M. Z. 2009 Solution of the parallel shear layer Green's function using conservation equations. *Intl J. Aeroacoust.* **8** (6), 585–602.

Afsar, M. Z. 2010 A complete theoretical foundation for the 'two-source' structure of jet noise. In *International Congress of Mathematicians*, Hyderabad, India.

Ahuja, K. K. 1973 Correlation and prediction of jet noise. *J. Sound Vib.* **25**, 155–168.

Alper, A. & Liu, J. T. C. 1978 On the interactions between large-scale structure and fine-grained turbulence in a round jet II. *Proc. R. Soc. Lond.* A **359**, 497.

Anderssen, N. 2003 A study of Mach 0.75 jets and their radiated sound using large-eddy simulation. PhD thesis, Chalmers University of Technology, Department of Thermo and Fluid Dynamics, Record No 16272.

Balsa, T. F. 1977 The acoustic field of sources in a shear flow with application to jet noise: convective amplification. *J. Fluid Mech.* **79**, 33–47.

Batchelor, G. K. 1953 *The Theory of Homegenous Turbulence*. Cambridge University Press.

Bishop, K. A., Ffowcs-Williams, J. E. & Smith, W. 1971 On the sources of the unsuppressed high-speed jet. *J. Fluid Mech.* **50**, 21–31.

Bodony, D. J. 2004 Aeroacoustic prediction of turbulent free shear flows. PhD thesis, Stanford University, Department of Aeronautics and Astronautics, Thesis Call No 3781 2005 B.

Bodony, D. J. 2009 Heating effects on the structure of noise sources of high-speed jets. In *47th Aerospace Sciences Meeting*, AIAA 2009-291, Orlando, FL.

Bodony, D. J. & Lele, S. K. 2005 Generation of low-frequency sound in turbulent jets. In *12th AIAA/CEAS Conference*, Monterey, CA.

Bodony, D. J. & Lele, S. K. 2008 Low-frequency sound sources in high-speed turbulent jets. *J. Fluid Mech.* **617**, 231–253.

Colonius, T. & Freund, J. B. 2000 Application of Lighthill's equation to a Mach 1.92 turbulent jet. *AIAA J. Tech. Notes* **38** (2) 368–370.

Colonius, T. & Lele, S. K. 2004 Computational aero-acoustics: progress on non-linear problems of sound generation. *Prog. Aerosp. Sci.* **40**, 345–416.

Colonius, T., Lele, S. K. & Moin, P. 1997 Sound generation in a mixing layer. *J. Fluid Mech.* **330**, 375–409.

Crighton, D. G. 1969 The scale effect in compressible turbulence. *Proc. Camb. Phil. Soc.* **65**, 557–565.

Crighton, D. G. 1993 Computational aero-acoustics for low Mach number flows. In *Computational Aero-Acoustics* (ed. J. C. Hardin & M. Y. Hussaini), pp. 50–68. Springer.

Crighton, D. G., Dowling, A. P., Ffowcs-Williams, J. E., Heckl, W. & Leppington, F. 1992. *Modern Methods in Analytical Acoustics*. Springer.

Crow, S. C. 1970 Aerodynamic sound emission as a singular perturbation problem. *Stud. Appl. Math.* **49** (1), 21–44.

Crow, S. C. 1972 The acoustic gain of a turbulent jet. *Bull. Am. Phys. Soc.* Paper IE. 6.

Dowling, A. P., Ffowcs-Williams, J. E. & Goldstein, M. E. 1978 Sound production in a moving stream. *Proc. R. Soc.* A **288**, 321–349.

Feynman, R. P., Leighton, R. B. & Sands, M. 1964. *The Feynman Lectures on Physics: Volume 1*. Addison-Wesley Longman.

Ffowcs-Williams, J. E. & Kempton, A. J. 1978 The noise from the large scale structure of a jet. *J. Fluid Mech.* **84**, 673–694.

Freund, J. B. 2001 Noise sources in a low-Reynolds-number turbulent jet at Mach 0.9. *J. Fluid Mech.* **438**, 277–305.

Freund, J. B. 2003 Noise source turbulence statistics and the noise from a Mach 0.9 jet. *Phys. Fluids* **15**, 1788–1800.

Goldstein, M. E. 1975 The low frequency sound from multipole sources in axisymmetric shear flows with application to jet noise. *J. Fluid Mech.* **70**, 595–604.

Goldstein, M. E. 1976 *Aero-Acoustics*. McGraw-Hill.

Goldstein, M. E. 1982 High frequency sound emission from moving point multipole sources embedded in arbitrary transversely sheared mean flows. *J. Sound Vib.* **80**, 499–521.

Goldstein, M. E. 1984 Aero-acoustics of turbulent shear flows. *Ann. Rev. Fluid Mech.* **16**, 263–285.

Goldstein, M. E. 2002 A unified approach to some recent developments in jet noise theory. *Intl J. Aeroacoust.* **1**, 1–16.

Goldstein, M. E. 2003 A generalized acoustic analogy. *J. Fluid Mech.* **488**, 315–333.

Goldstein, M. E. 2005 Ninety degree acoustic spectrum of a high speed air jet. *AIAA J.* **43**, 96–102.

Goldstein, M. E. & Leib, S. J. 2005 The role of instability waves in predicting jet noise. *J. Fluid Mech.* **525**, 37–72.

Goldstein, M. E. & Leib, S. J. 2008 The aero-acoustics of slowly diverging supersonic jets. *J. Fluid Mech.* **600**, 291–388.

Huerre, P. & Crighton, D. G. 1983 Sound generation by instability waves in a low Mach number jet. *AIAA Paper* 83-0661.

Karabasov, S. K., Afsar, M. Z., Hynes, T. P., Dowling, A. P., McMullen, W. A., Pokora, C. D., Page, G. J. & McGuirk, J. J. 2010 Jet noise-acoustic analogy informed by large eddy simulation. *AIAA J.* **48** (7).

Lebedev, N. N. 1972 *Special Functions and Their Applications.* Dover.

Lighthill, M. J. 1952 On sound generated aerodynamically. Part I. General theory. *Proc. R. Soc.* A **222**, 564–587.

Lilley, G. M. 1958 On the noise from air jets. *ARC-20, 376, No. 40, Fm-2724*, British Aeronautical Research Council.

Lilley, G. M. 1974 On the noise from jets. *CP-131* AGARD, 13.1–13.12.

Liu, J. T. C. & Mankbadi, R. 1984 Sound generated aerodynamically revisited: large-scale structures in a turbulent jet as a source of sound. *Proc. R. Soc. Lond.* A **311** (1516), 183–217.

Liu, J. T. C. & Merkine, L. 1976 On the interactions between large-scale structure and fine-grained turbulence in a round jet. Part I. *Proc. R. Soc. Lond.* A **352**, 213.

Lush, P. A. 1971 Measurements of subsonic jet noise and comparison with theory. *J. Fluid Mech.* **46**, 477–500.

Mollo-Christensen, E., Koplin, M. A. & Martucelli, J. R. 1964 Experiments on jet flows and jet noise, far-field spectra and directivity patterns. *J. Fluid Mech.* **18**, 285–301.

Moore, P. D., Slot, H. J. & Boersma, B. J. 2007 Direct numerical simulation of low Reynolds number hot and cold jets. In *13th AIAA/CEAS Aero-Acoustics Conference*, Rome, Italy.

Morris, P. J. 2008 Source modelling and prediction methodologies. In *ERCOTAF Symposium on Sound Source Mechanisms in Turbulent Shear Flow,* Poiters, France, July 7–9, 2008.

Morris, P. J. 2009 A note on noise generation by large scale turbulent structures in subsonic and supersonic jets. *Intl J. Aeroacoust.* **8**, 4, 301–316.

Morris, P. J. & Farrasat, F. 2002 Acoustic analogy and alternative theories for jet noise prediction. *AIAA J.* **40**, 671–680.

Morse, P. M. & Feshbach, H. 1953 *Methods of Theoretical Physics, Part I.* McGraw-Hill.

Mosedale, A. & Drikakis, D. 2007 Assessment of very high order of accuracy in LES models. *ASME J. Fluids Engng* **129**, 1497.

Nayfeh, A. H. 1972 *Perturbation Methods.* Wiley Interscience.

Power, O., Kerherve, F., Fitzpatrick, J. & Jordan, P. 2004. Measurements of turbulence statistics in high Reynolds number jets. In *10th AIAA/CEAS Aero-Acoustics Conference*, Manchester, UK.

Ribner, H. S. 1969 Quadrupole correlations governing the pattern of jet noise. *J. Fluid Mech.* **38**, 1–24.

Shur, M. L., Strelets, M. Kh. & Spalart, P. R. 2007. Numerical system for LES-based jet noise prediction: validation and application to evaluation of noise-reduction concepts. In *West East High Speed Flow Conference*, Moscow, Russia.

Stromberg, J. L., McLaughlin, D. K. & Troutt, T. R. 1980 Flow field and acoustic properties of a Mach 0.9 jet at a low Reynolds number. *J. Sound Vib.* **72**, 159–176.

Tam, C. K. W. 1971 Directional acoustic radiation from a supersonic jet generated by shear layer instability. *J. Fluid Mech.* **46**, 757–768.

Tam, C. K. W. 1995 Supersonic jet noise. *Ann. Rev. Fluid Mech.* **27**, 17–43.

Tam, C. K. W. & Auriault, L. 1998 Mean flow refraction effects on sound radiated from localized sources in a jet. *J. Fluid Mech.* **370**, 149–174.

Tam, C. K. W. & Auriault, L. 1999 Jet mixing noise from fine scale turbulence. *AIAA J.* **206**, 145–153.

Tam, C. K. W. & Burton, D. E. 1984 Sound generated by instability waves of supersonic flow. Part 2. Axi-symmetric jets. *J. Fluid Mech.* **138**, 273–295.

Tam, C. K. W., Viswanathan, K., Ahuja, K. K. & Panda, J. 2008 The sources of jet noise: experimental evidence. *J. Fluid Mech.* **615**, 253–292.

Wang, M., Freund, J. B. & Lele, S. K. 2006 Computational prediction of flow generated sound. *Ann. Rev. Fluid Mech.* **38**, 483–512.

Wu, X. & Huerre, P. 2009 Low frequency sound radiated by a non-linearly modulated wavepacket of helical modes on a subsonic circular jet. *Fluid Mech.* **637**, 173–211.

Wu, X., McGuirk, J. J., Tristanto, I. H. & Page, G. J. 2005 Influence of nozzle modelling in LES of turbulent free jets. In *11th AIAA/CEAS Aero-Acoustics Conference*, Monterey, CA.